Geomorphology 400 (2022) 108096

Contents lists available at ScienceDirect

Geomorphology

journal homepage: www.elsevier.com/locate/geomorph

De-icing landsystem model for the Universidad Glacier (34° S) in the Central Andes of Chile during the past ~660 years

Hans Fernández [a,*], Juan-Luis García [a,b], Samuel U. Nussbaumer [c,d], Alessa Janine Geiger [a], Isabelle Gärtner-Roer [c], Francia Pérez [a], Dmitry Tikhomirov [c], Marcus Christl [e], Markus Egli [c]

[a] Pontificia Universidad Católica de Chile, Instituto de Geografía, Santiago, Chile
[b] Centro UC Desierto de Atacama, Pontificia Universidad Católica de, Chile
[c] University of Zurich, Department of Geography, Zürich, Switzerland
[d] University of Fribourg, Department of Geosciences, Fribourg, Switzerland
[e] Institute of Ion Beam Physics, ETH, Zürich, Switzerland

ARTICLE INFO

Article history:
Received 12 July 2021
Received in revised form 23 December 2021
Accepted 24 December 2021
Available online 2 January 2022

Keywords:
Latest Holocene
Debris-covered glaciers
Ice-cored moraine
Glacial geochronology
Paraglacial

ABSTRACT

Reconstructing latest Holocene (<1000 years) glacial landscape development in the Central Andes of Chile (30–35° S) is key for understanding the response of the cryosphere during periods of negative glacier mass balance, such as the current one. The excellently preserved glacial landscape produced during the latest ice advance and retreat cycle is of particular interest for examining the detailed response of glaciers to deglaciation. To establish a conceptual model of glacier behavior under warm and dry climatic conditions, we reconstructed and dated the recent glacial history of the Universidad Glacier (34° S) through detailed geomorphological mapping and ^{10}Be cosmogenic surface exposure dating. Our mapping describes a landsystem that spans from the current ice front to ~3 km down-valley, where a mosaic of glacial landforms includes mounded relief; sinkholes; debris-filled stripes; moraine belts; flutings; and a prominent basal till plain. Our ^{10}Be ages suggest that the Universidad Glacier has fluctuated in its forefield since the 13th – 15th centuries CE. We propose that the glacier evolved from a clean glacier to a debris-covered glacier, to an ice-cored moraine, and finally, to a massive dead-ice topography. This deglacial evolution intermittent and potentially reset by multiple standstills and/or re-advances during the overall retreat. The implication is that phases of active ice were followed by stagnation associated with progressive melting of dead ice under the supraglacial debris layer. Similar geomorphic features and processes are recorded in the present-day Universidad Glacier ablation zone, denoting a recurrent reconditioning over time analogous to the glacier's evolution during the latest Holocene.

1. Introduction

Glacial landforms in high mountains are unique indicators of morphogenetic processes linked to distinct glacial dynamics and climatic fluctuations (Benn and Evans, 2014; Mackintosh et al., 2017). Despite the existence of well-preserved Holocene glacial landforms in the Central Andes of Chile (30–35°S), only a few studies have aimed at understanding the geomorphological transition from glacial to non-glacial landscapes in response to climate warming (Bodin et al., 2010; García et al., 2014; Janke et al., 2015; Monnier and Kinnard, 2017; Iturrizaga and Charrier, 2021). Notable unresolved questions include:

- What are the geomorphic processes that occur during warm and dry periods in a glaciated basin of the Central Andes of Chile?
- Do glacier fronts retreat abruptly or by progressive de-icing with standstills and/or re-advances phases during the overall deglaciation?
- Is it possible to define a latest Holocene deglaciation landsystem model for a prominent glacier system in the Central Andes of Chile based on geomorphic records?

In this paper, we aim to build a conceptual model of deglaciation that better characterizes the response of glaciers to warm and dry periods in the Central Andes of Chile. Our model is based on detailed geomorphic mapping of the latest Holocene glacier record constrained by ^{10}Be exposure dating in the forefield of the Universidad Glacier (34° 42′ S, 70° 20′ W). This approach provides temporal context for the deglaciation of the 20th and 21st centuries and insights into the long-term deglacial process for this mountain area. Our study area in the hinterland of the most populated area in Chile represents one of the chief sources of freshwater for human and agricultural uses (Bellisario et al., 2013;

* Corresponding author.
E-mail address: hdfernandez@uc.cl (H. Fernández).

https://doi.org/10.1016/j.geomorph.2021.108096
0169-555X/

Ayala et al., 2016). Understanding the response of local glaciers to climate change is essential for sustainable water planning.

1.1. Conceptual models of de-icing

Geomorphological processes related to ice melting are enhanced in high mountains. In these areas, the deglacial process that follows a glacial expansion includes a long-term period of sediment and geomorphic adjustment (Ballantyne, 1995, 2002, 2008; Benn and Owen, 2002; Evans and Twigg, 2002; Curry et al., 2006) characterized by a high rate of debris mobilization and deposition at the lower margin of glaciers due to negative mass balance and ice stagnation (Eyles, 1979; Kjær and Krüger, 2001; Lukas et al., 2005, 2007; Schomacker, 2007; Evans, 2014). The debris generally comes from mass movement of ice-free adjacent valley slopes (Eyles and Rogerson, 1978; Eyles, 1979; Curry et al., 2006; Evans, 2009; Eichel et al., 2018) or avalanches (Owen, 1991; Shroder et al., 2000; Hambrey et al., 2008). Englacial debris accumulates on the glacier surface when the ice is thinning (Janke et al., 2015). In the transition between the active glacier and the stagnant snout, subglacial sediments can be thrust up to the supraglacial environment (Glasser and Hambrey, 2002; Swift et al., 2018).

Geomorphological models of deglaciation have been constructed for the Andes, Himalayas, and Europe to understand the current de-icing process. According to Janke et al. (2015), the present-day evolution of glacial landscapes in the Central Andes of Chile could be better understood as a continuous transition from clean to debris-covered glaciers and, possibly, glaciogenic rock glaciers. Complementarily, García et al. (2014) suggested that a transitional state from clean glaciers to debris-covered glaciers may be ice-cored moraines: buried bodies of ice detached from the active or stagnant glacier up-valley (Kjær and Krüger, 2001; Lukas et al., 2007; Evans, 2014). In both cases, ice melt produces an upper layer of rock material that mostly insulates underlying ice (García et al., 2014; Janke et al., 2015). In the Himalayas, Shroder et al. (2000) suggested that the transition from debris-covered glaciers to rock glaciers depends on the sediment transfer rate from ablation zones to glaciofluvial systems. An inefficient transfer would thicken the supraglacial layer, increasing the insulation of internal ice (Shroder et al., 2000; Jones et al., 2019). Other investigations in Central Asia found that the main causes of mass loss in debris-covered snouts are supraglacial melt-out ponds and ice cliffs (Sakai et al., 2000; King et al., 2020; Buri et al., 2021). In this manner, surface lowering is associated with the development and subsequent degradation of dead-ice zones (Benn and Owen, 2002).

In Europe, the degradation of ice-cored moraines has been well-established. Backwasting of the ice front and glacier downwasting become a significant cryogeomorphic process during warm periods (Kjær and Krüger, 2001; Krüger et al., 2010; Reid and Brock, 2014). The variable thickness of the glacier's debris cover results in differential downwasting rates in the ablation area, producing a hummocky topography (Patterson, 1998; Schomacker, 2008; Evans, 2009; Oliva and Ruiz-Fernández, 2015). Features associated with a karstic evolution on stagnant ice may be identifiable, such as funnel-shaped sinkholes (*sensu* Clayton, 1964; Kjær and Krüger, 2001; Schomacker and Kjær, 2008) and debris-filled stripes, which are produced from tension cracks (Eyles, 1979; Kjær and Krüger, 2001). Complete de-icing of the ice-cored moraines results in a dead-ice moraine with massive ice-free hummocky topography (Kjær and Krüger, 2001; Schomacker and Kjaer, 2007; Krüger et al., 2010).

Debris-covered glacier de-icing models contrast inactive ice at the terminus with active flowing ice up-valley in the same glacier tongue (Kjær and Krüger, 2001; García et al., 2014; Phillips et al., 2017). This results in a stationary ice front, unlike the retreating ice front typical of clean mountain glaciers during negative mass balance periods (Bennett et al., 2000; Krüger et al., 2010).

2. Regional setting

The highest peaks in the Central Andes of Chile reach ~6000 m a.s.l (Fig. 1a). The Andes' rugged topography is characteristic of active tectonic uplift, volcanism, and incised glacial basins (García et al., 2014; Charrier et al., 2019). Its altitude and physical setting promote different sizes and types of glaciers (Lliboutry, 1998), such as clean glaciers; clean glaciers with debris-covered snouts; debris-covered glaciers; and rock glaciers. Clean glaciers and debris-covered glaciers are more common to the south of 33° S, while rock glaciers dominate the North (Azócar and Brenning, 2010).

The entire glacier-covered area in the Central Andes of Chile has been shrinking dramatically since at least the middle of the 20th century (Barcaza et al., 2017). Between 2000 and 2019, an accelerated loss of glacier mass has been observed (Hugonnet et al., 2021). Moreover, the present mega-drought in central Chile is the longest dry period in the last millenium (Garreaud et al., 2020). Malmros et al. (2016) confirmed a total reduction of the exposed ice area in the Central Andes of Chile and Argentina (32°–33° S) from 134 to 94 km^2 between 1955 and 2014. The loss of glaciated area and projections for a warmer climate have turned attention to debris-covered glaciers and rock glaciers as important regional water resources (Azócar and Brenning, 2010; Bellisario et al., 2013; Janke et al., 2015; Fernández and Ferrando, 2018).

The Central Andes of Chile are south of the Pacific side of the Arid Diagonal (Abraham et al., 2020). In this region, winter precipitation produced by the southern westerlies dominates (Garreaud, 2009). 80% of the annual precipitation occurs between May and August, mostly in the form of snow. According to regional climate data from the Embalse El Yeso station (33° 40′ S, 70° 5′ W, ~2400 m a.s.l.), the mean annual air temperature is 8.3 °C and the mean annual precipitation is 515 mm (Barcaza et al., 2017). The local climate defines the equilibrium line altitude (ELA) of the glaciers at 4300–4400 m a.s.l. in the north, declining gradually to 3200 m a.s.l. south of 33° S (Brenning, 2005; Azócar and Brenning, 2010).

The Universidad Glacier is surrounded by high summits. The highest peaks on the west side of the catchment area include Cerro Alto Los Arrieros (4990 m a.s.l.), El Portillo (4957 m a.s.l.), and Cerro El Brujo (4458 m a.s.l.). To the east, the highest peaks include the volcano El Palomo (4860 m a.s.l.) and other peaks at ~3500 m a.s.l. El Palomo has no volcanic activity at present. The main lithologies surrounding the Universidad Glacier are granodiorites, rhyolites and andesites (Charrier and Lillo, 1973) (Fig. 1b).

The mountain range that surrounds the Universidad Glacier also hosts three other glaciers that, together, cover an area of ~50 km^2 (Dirección General de Aguas, 2014): Cipreses Glacier to the northwest, Cortaderal Glacier to the east, and Palomo Glacier to the north (Fig. 1b). The Universidad Glacier has the largest surface area in the Central Andes of Chile, 28.1 km^2 (Wilson et al., 2016), and a notable length of ~10 km. The Universidad Glacier originates from the El Palomo volcano and merges down-valley with Manke Glacier (Fig. 1c). At present, the Universidad Glacier flows down-valley from 4540 to ~2500 m a.s.l (Le Quesne et al., 2009). Aerial photographs available since 1944 allow tracing the evolution of the ice front since then. In the 1944 Trimetrogon

Fig. 1. Location of the **study area in the Central Andes of Chile** (30–35°S). **(a)** Location of the study area in South America and the Central Chile. Main cities near the Universidad Glacier are marked with yellow stars; **(b)** The glacier inventory (Dirección General de Aguas, 2014) and the geological setting of the study area, with reconstructed Pleistocene and Holocene moraines (red lines) mapped along the Universidad Glacier valley; **(c)** Universidad Glacier and the latest Holocene UNI V moraine complex (white dotted line) and moraine ridges (black lines); **(d)** The oldest historical imagery of the Universidad Glacier from 1944 with view to the west.

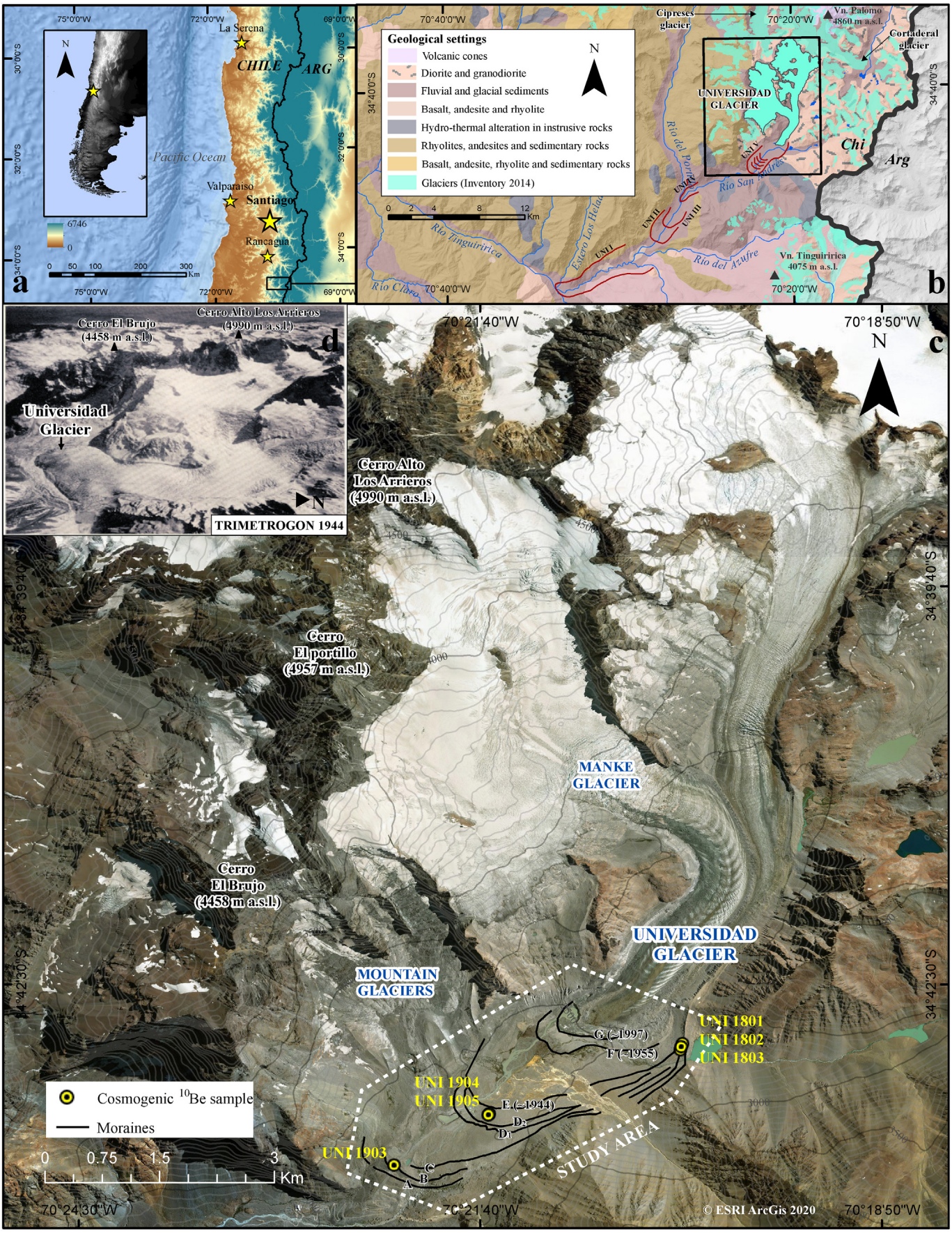
a
La Serena
CHILE
ARG
Pacific Ocean
Valparaiso
Santiago
Rancagua
b
Geological settings
Volcanic cones
Diorite and granodiorite
Fluvial and glacial sediments
Basalt, andesite and rhyolite
Hydro-thermal alteration in instrusive rocks
Rhyolites, andesites and sedimentary rocks
Basalt, andesite, rhyolite and sedimentary rocks
Glaciers (Inventory 2014)
Cipreses glacier
Vn. Palomo 4860 m a.s.l.
Cortaderal glacier
UNIVERSIDAD GLACIER
Río del Portillo
Río San Andres
Chi
Arg
Río Tinguiririca
Estero Los Helados
Río del Azufre
Vn. Tinguiririca 4075 m a.s.l.
Río Claro
d
Cerro El Brujo (4458 m a.s.l.)
Cerro Alto Los Arrieros (4990 m a.s.l.)
Universidad Glacier
TRIMETROGON 1944
c
Cerro Alto Los Arrieros (4990 m a.s.l.)
Cerro El portillo (4957 m a.s.l.)
MANKE GLACIER
Cerro El Brujo (4458 m a.s.l.)
UNIVERSIDAD GLACIER
MOUNTAIN GLACIERS
UNI 1801
UNI 1802
UNI 1803
G (≃1997)
F (≃1955)
UNI 1904
UNI 1905
E (≃1944)
D2
D1
UNI 1903
C
B
A
STUDY AREA
Cosmogenic 10Be sample
Moraines
0 0.75 1.5 3 Km
© ESRI ArcGis 2020

aerial photographs, the ice front was 1.5 km further down-valley than at present (Fig. 1d). Between 1944 and 1955, the ice front retreated 1 km (HYCON flight, 1955). Since 1955, the ice front has retreated about 300 m.

3. Materials and methods

3.1. Geomorphological mapping

Our geomorphological mapping is based on interpretation of satellite images, field visits, and stereoscopic interpretation of aerial photographs. We analyzed aerial photos from 1997 (1:50,000, produced by GEOTEC flight, Servicio Aerofotogramétrico (SAF), Chile) and 1955 (1:70,000, produced by HYCON flight, SAF Chile). We acquired recent terrain imageries from GeoEye (2015), DigitalGlobe (2018), and ESRI ArcGIS (2020). We composited a Digital Elevation Model (DEM) with 12.5 m resolution from ALOS-PALSAR data (https://vertex.daac.asf.alaska.edu/). In addition, we retrieved geological data from national and regional geological databases to compile a map (1:500,000) (Charrier and Lillo, 1973; SERNAGEOMIN, 2004) (Fig. 1b).

Once we identified main glacial features through geomorphological mapping on remotely sensed data, we carried out three fieldwork campaigns (in January and April of 2019 and January of 2020, for a total of 30 days) to check and improve the remotely mapped glacial geomorphology. The terminal glacier zone, the upper ablation zone, and the glacier forefield were explored extensively. We used a handheld GPS device with ±3 m horizontal accuracy to document sample and landform locations. We used ESRI ArcGIS 10.3 to produce our geomorphic maps, applying the glacial geomorphology symbology of Barsch and Liedtke (1980) and Kneisel (1988).

3.2. Geochronology

To establish a general geochronological time frame, we collected rock samples (>1.5 kg) from the top (upper <2 cm) of six granodiorite boulders (Table 1; Supplementary Material) resting on moraine ridges and flute fields for *in situ* terrestrial cosmogenic nuclide dating (TCND, ^{10}Be), following standard procedures (Gosse and Phillips, 2001). The sampling focused on boulders ranging in size between 90 and 240 cm above the surrounding surface with minimal surface weathering, fractures, or evidence of gravitational movement or post-depositional exhumation. Each boulder had glacial erosional features such as striations (Supplementary Material). We collected rock samples with a hammer and chisel, blasts, and a handheld circular saw. Clean quartz was extracted at the Pontificia Universidad Católica de Chile - Cosmogenic Isotope Laboratory, while Beryllium was isolated at the Surface Exposure Lab at the University of Zürich, following a procedure adapted from Kohl and Nishiizumi (1992). All ^{10}Be/^{9}Be ratios were measured at the ETH Zurich Tandy AMS system (Christl et al., 2013) and normalized to the ETH in-house AMS standards S2007N and S2010N (^{10}Be/^{9}Be = $28.1\cdot10^{-12}$ and $3.3\cdot10^{-12}$, respectively), which were calibrated to the ICN 01–5-1 standard (Nishiizumi et al., 2007). All AMS standards are associated with a ^{10}Be half-life of 1.387 ± 0.012 Myr (Chmeleff et al., 2010; Korschinek et al., 2010). ^{10}Be/^{9}Be sample ratios were corrected with the weighted average of the two chemistry blanks (Table 1; Supplementary Material). We calculated ^{10}Be exposure ages with the CRONUS-Earth online calculator (http://hess.ess.washington.edu/math/) version 3 (Balco et al., 2008). We used the local calibration dataset developed by Kaplan et al. (2011) to obtain the ^{10}Be production rate for southern South America. The calibration data was obtained from the online ICE-D platform (http://calibration.ice-d.org/). We excluded both erosion and shielding by snow and/or sediment from the exposure age calculations due to the boulders' visible striations, indicating low surface weathering rates from the time of deposition. The height of the sampled boulders above the surrounding topography makes snow/sediment shielding less likely. It is also very difficult to determine

Table 1
Geographical, analytical, and exposure ages data of ^{10}Be samples in the forefield of the Universidad Glacier.

Sample name	Latitude (DD)	Longitude (DD)	Elevation (m a.s.l.)	Type of sample	Sample height (cm)	Shielding factor	Sample thickness (cm)	Quartz dissolved (g)	^{9}Be carrier added (mg)	^{10}Be/^{9}Be AMS ratio (10^{-14})	Error ^{10}Be/^{9}Be (10^{-12})	^{10}Be (at/g) (x10^{4})	Error ^{10}Be conc. (10^{3}) (at/g)	Error (%) ^{10}Be (at/g)	Exposure Age (years before present)
UNI 1801	−34.715968	−70.337477	2625	Erratic embedded in lateral ridge of moraine B	124	0.977921	2.6	54.34	0.2044	1.562	0.003	0.3925	0.68	17.3	**240 ± 40**
UNI 1802	−34.715601	−70.337388	2625	Erratic embedded in lateral ridge of moraine B	118	0.977336	1.9	60.67	0.2037	2.383	0.003	0.5347	0.78	14.6	**330 ± 50**
UNI 1803	−34.715239	−70.337252	2626	Erratic in lateral ridge of moraine B	90	0.975470	1.8	49.60	0.1989	4.344	0.010	1.1641	2.5	21.9	**665 ± 150**
UNI 1903	−34.729639	−70.371167	2355	Erratic on frontal ridge of moraine B	240	0.959408	1.3	30.56	0.2046	1.477	0.003	0.6607	1.36	20.7	**470 ± 100**
UNI 1904	−34.723556	−70.359944	2436	Embedded boulder in flute field between moraines D_2 and E	103	0.969602	1.6	55.29	0.2045	2.123	0.003	0.5248	0.69	13.1	**360 ± 50**
UNI 1905	−34.723694	−70.360056	2430	Superimposed boulder on flute field between moraines D_2 and E	103	0.972656	1.7	50.21	0.2029	2.519	0.006	0.6802	1.55	22.9	**460 ± 100**
UNI BI 11				Chemistry blank					0.2037	0.014*	0.002*				
UNI BI 12				Chemistry blank					0.2022	0.009**	0.002*				

Note: ^{10}Be ages were calculated using the CRONUS-Earth online calculator (http://hess.ess.washington.edu/math/) version 3, wrapper script & get age: 3.0.2, muons: 1A, alpha = 1, constants: 2020-08-26 using the 07KNSTD standardization (Balco et al., 2008; Nishiizumi et al., 2007). Exposure ages are provided in the "Lm" time-dependent scaling scheme using standard atmospheric pressure (Lal, 1991; Stone, 2000). All ages are calculated with the local ^{10}Be production rate for southern South America (Kaplan et al., 2011). We use a sample rock density of 2.65 g/cm^3 and apply no erosion correction. Reported ^{10}Be/^{9}Be ratio for 07KNSTD is $2.85\cdot10^{-12}$ (Nishiizumi et al., 2007). The ^{9}Be/^{10}Be sample ratio was corrected with the weighted average of the blank ratios.

* Blank ratios are presented without correction to the weighted average of blanks.

** Be ratio of the AMS determined directly by the blanks.

snow cover density and duration; therefore, our exposure ages should be regarded as minimum ages. All exposure ages reported here are in the ^{10}Be time-dependent scaling scheme (Lm) after Lal (1991) and Stone (2000) (Table 1). Outputs from other scaling schemes do not change the final interpretations of exposure ages presented here.

4. Results

4.1. Geomorphology of the glacier forefield

The Universidad Glacier valley has four distinct moraines within a distance of 20 km, located between 1000 and 2500 m a.s.l. We labeled them from outer to inner as UNI I to UNI IV (Fig. 1b). UNI IV, the latest Holocene moraine complex, extends ~3 km down-valley from the ice front (Fig. 2), covering the present-day forefield. The UNI IV moraine complex includes different types of glacial landforms and structures punctuated by eight moraine ridges.

4.1.1. Moraine ridges

Eight moraine ridges (A-G from distal to proximal) occur in UNI IV between the current glacier margin and a ~45° steep and ~400 m high topographic step 3 km down-glacier (Fig. 2). The outermost frontal moraine A was deposited over gently sloping terrain, where rounded and sub-rounded boulders, some well-faceted and -striated, occur (Fig. 3a). This diamictic terrain seems to be older than the moraine ridge A.

In some cases, the moraine ridges can be tracked all along the eastern lateral and frontal margins (Fig. 2). The moraines in the southwest part of the valley have been crosscut and/or overridden by advances of the mountain glaciers from Cerro El Brujo and their preservation is less clear (Figs. 1, 2). The eastern lateral moraines A-D, near the glacier front, exhibit a stepped sequence (Fig. 4a). The proximal slopes of these moraines vary between ~15° and ~40°, with the higher angles in the outer moraines A and B. These outer moraines comprise mainly angular and sub-angular, but also sub-rounded boulders. Moraines C and D are formed by matrix-supported diamicts. Some distal sections of the external lateral moraines have been partly covered by colluvial sediment (Fig. 4a). Erosive debris flows have interrupted the continuity of the eastern lateral sections of moraines A-D (Fig. 2).

The frontal sections of moraines A-D remain well-preserved and are relatively similar in height (~5 m). Their lithologic composition is mostly granodiorite, with a proximal slope angle of 20 to 30° and sub-angular to angular boulder roundness. The frontal margins of moraines A-B are 90–100 m apart from each other. Both ice-marginal positions are separated by a conspicuous deposit of angular basaltic boulders (Fig. 3b). Moraine C is located 130 m up-valley from moraine B, which was crosscut by a mountain glacier expansion from Cerro El Brujo (Figs. 1c, 2). Between moraines B and C, scattered boulders and patches of sand of varying shapes and sizes make up an irregular terrain. The largest sandy patch has a basaltic and quartz lithology and is in the central part of the valley in front of moraine C, with a length of ~50 m and a

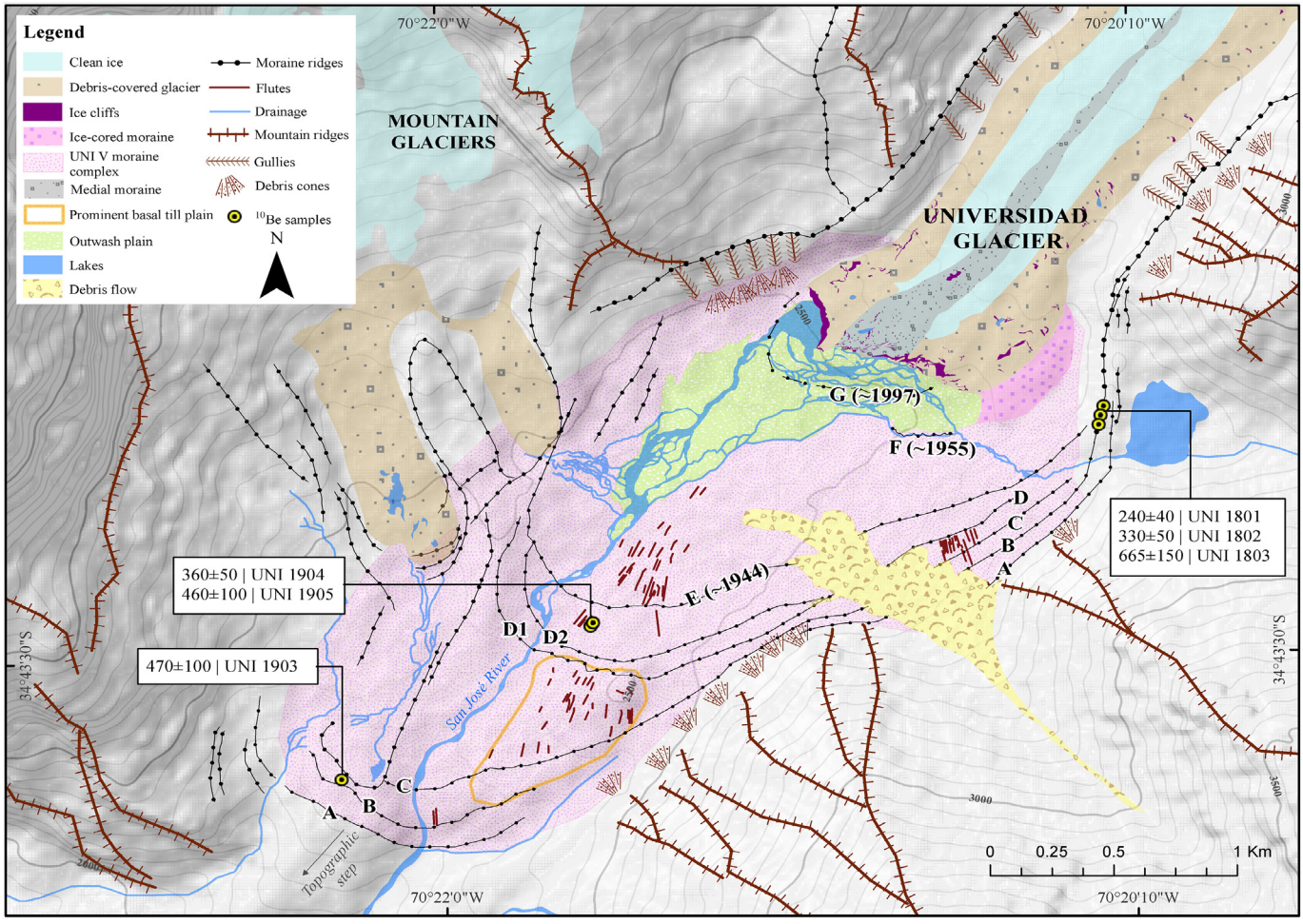

Fig. 2. Glacial geomorphology and geochronology of the Universidad Glacier forefield. Dotted lines represent the moraine ridges, labeled A – G. On moraine B and between moraines D-E, rock samples were obtained to measure the ^{10}Be exposure surface dates that offer a temporal frame of the landscape evolution. Moraines A-C represent the outer ice extent of UNI V moraine complex; D_1-E represent the extensive ice, until, at least, the first half of the 20th century; F-G denote much less prominent glacier over the middle and the end of the 20th century. The current glacier front is almost completely covered with debris.

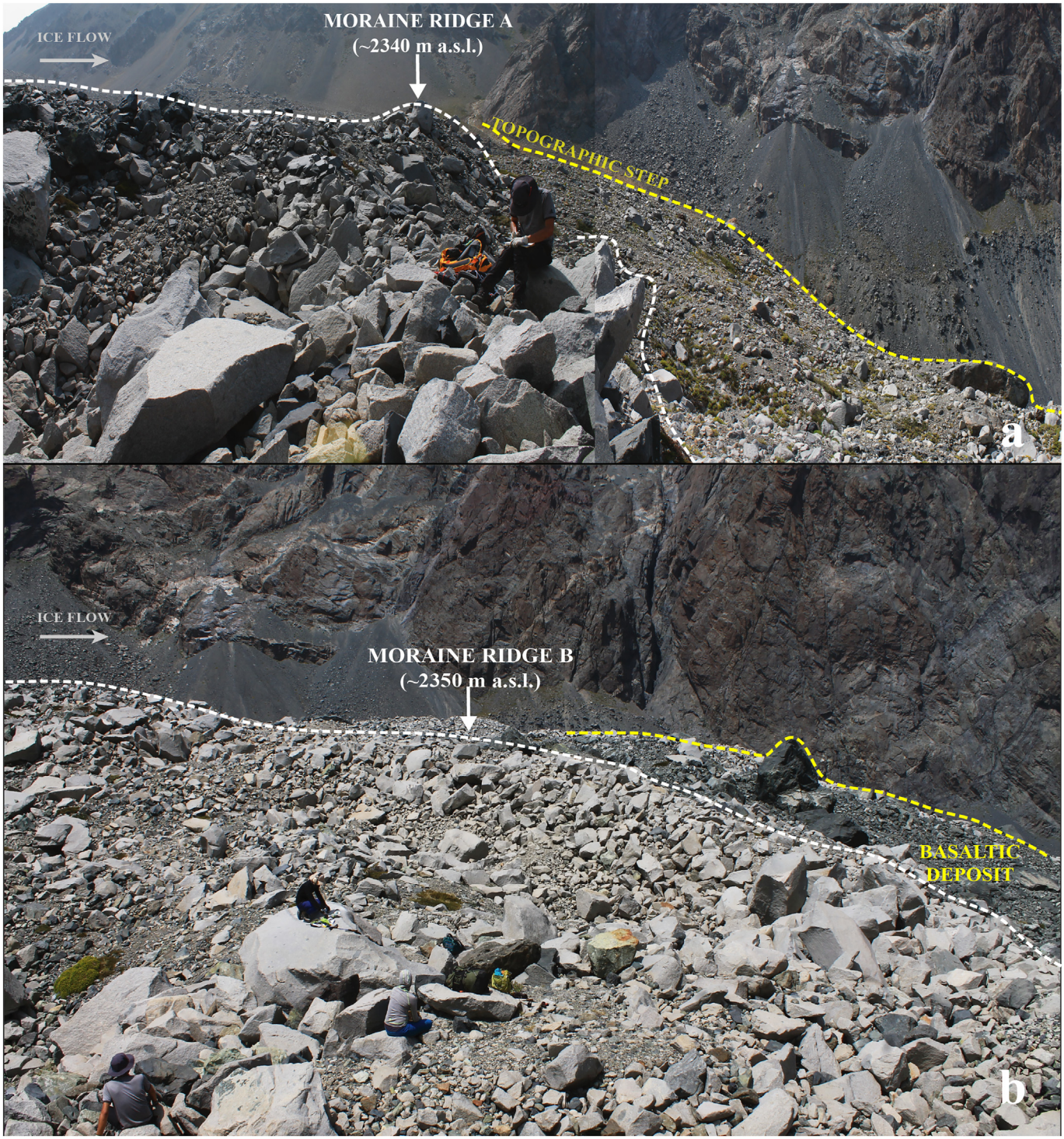

Fig. 3. Frontal ridges of moraines A and B. (a) The frontal ridge of moraine A is composed mainly of angular boulders. The moraine grades towards a topographic step with striking widespread well-polished boulders that contrast with moraines A-B; **(b)** Intermorainal bouldery hummocky topography of moraines A and B, which includes a basaltic (volcanic) deposit. Ridge of moraine B is also pointed out.

width of ~30 m. The proximal terrain of moraine C reveals a paved surface with flutes (Fig. 2) (see section 4.1.3).

The frontal section of moraine D is 1.5 km down-valley from the ice margin on the proximal side of a prominent oval-shaped landform (Fig. 2) (see section 4.1.2). The crest splits into two sinuous ridges, D_1 and D_2, 10–20 m apart from each other (Fig. 4b). The intermorainal depression between moraines D_1 and D_2 is mainly sand, silt, and abandoned meltwater channels. Both moraine ridges are topped with polished and faceted boulders covered partly by a thin and patchy debris veneer. This debris cover is mainly sub-angular and sub-rounded cobbles. Between moraines D_2 and E, there is a set of well-preserved flutes (see section 4.1.3) (Fig. 2).

Moraine E is found 1.3 km from the ice front. The well-preserved morainic arc is uninterrupted over 2.5 km. It is composed mainly of sub-angular to sub-rounded boulders and cobbles, supporting faceted and striated embedded boulders. Moraine E coincides with the glacier position captured by the 1944 Trimetrogon aerial photograph (Fig. 1d). The inboard part of moraine E hosts flutes of different lengths and sizes (see

Fig. 4. Overview of the forefield and moraines D_1 and D_2. (a) Forefield from the top of basal till plain (oval-shaped landform) with the current glacier in the back. The view is towards the North. Eastern lateral ridges of moraines A-D are arranged in a staggered sequence, representing the outer ice-marginal position. Moraine E, which coincides approximately with the 1944 ice position in Trimetrogon aerial photograph, is a perfectly defined morainic arc. The upper left white arrow indicates the North; **(b)** Frontal moraine D is divided into two ridges (D_1 and D_2) deposited on the proximal side of the prominent basal till plain on the UNI V moraine complex. The upper left shows an alignment of debris in the ground on the prominent landform. At the bottom right are two orange tents in the hydropower station infrastructure for scale. The view is to the east.

section 4.1.3). Moraine F is a remarkable moraine located ~440 m from the glacier front (Fig. 5). It has a height of 7 m and is composed of distinct rounded granodiorite pebbles and boulders. On its top, some of these boulders are striated and faceted. It has a serpentine shape oriented east-west over 300 m. According to HYCON aerial photography, its position seems to indicate the 1955 latero-frontal ice margin. Lastly, moraine G occurs in patches of no more than 5 m in height on the active outwash plain and spreads out in a sinuous shape. This moraine is 300 m distal to the present glacier front (Fig. 5). Moraine G coincides with the 1997 ice front position captured by GEOTEC aerial photography.

In summary, the outer moraines (A, B, and C) are more prominent and well-preserved in their frontal and left lateral margins. They represent the outer ice extents of the UNI IV moraine complex. Moraines D_1-E denote the presence of extensive ice until at least the middle of the 20th

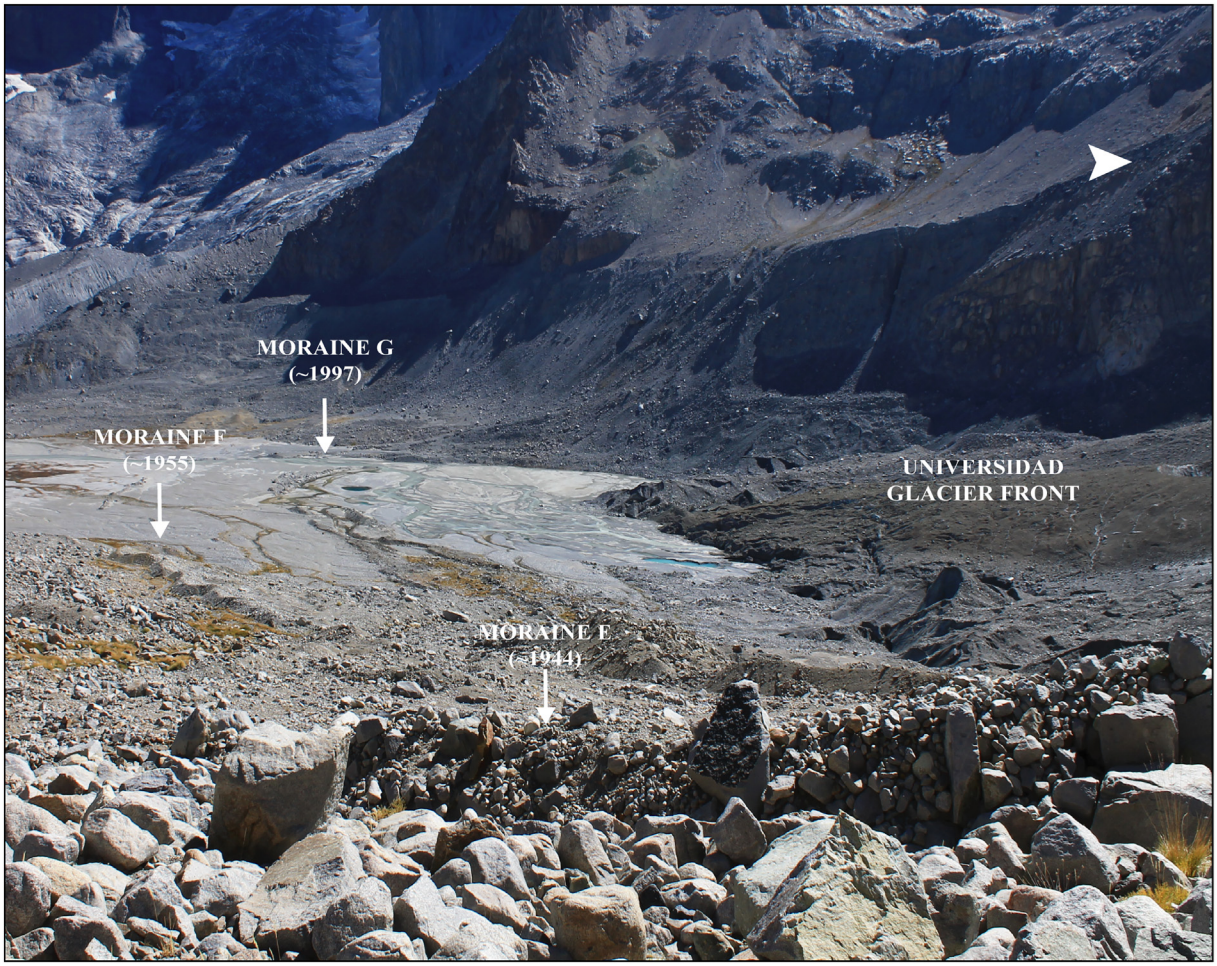

Fig. 5. Universidad Glacier front. The ice front is totally debris-covered and shows a gentle slope punctuated by ice cliffs and meltwater channels. In the foreground the ridge of moraine E (~1944). In the background, moraine F with a serpentine shape (~1955), and the moraine patches left from the ~1997 moraine (G). The upper right white arrow indicates the North.

century. Moraines F and G indicate a much less prominent glacier over the middle and end of the 20th century. Moraines A-G are distinct evidence of significant former marginal positions, except for moraine G, which is primarily mounds being eroded by meltwater streams in the outwash plain (Fig. 5).

4.1.2. Hummocky terrain

Moraines A-G are distributed over a massive hummocky terrain that covers most of the forefield, except for the active outwash plain (Fig. 2). The hummocky terrain is an irregular complex where the following coexist: i) an irregular bouldery topography; ii) rounded basins with an accumulation of debris at their bottom; iii) debris-filled stripes in the ground; iv) a prominent oval-shaped landform; and v) glacial lineations.

Large angular boulders (>3 m) are piled up between moraines A and C (Fig. 6a), while smaller sub-angular debris occurs inboard from moraine C (Fig. 6c-e). This produces an overall granulometric gradient along the hummocky terrain. Throughout the hummocky terrain, inactive sinkholes (Krüger et al., 2010; Schomacker, 2007) filled with debris at their bottoms have been identified. The largest sinkholes are in the outer area, with depths of >3 m and widths of >5 m (Fig. 6a). Here, recurrent sinkholes, one next to the other and separated by high ground, produce chaotic hummocky relief. In contrast, smaller sinkholes occur inboard to moraine C. The smaller sinkholes are 4–5 m wide and 2 m deep and also have debris accumulation at their bottoms (Fig. 6c).

Debris-filled stripes in the ground (Fig. 6b) cover most of the hummocky terrain complex, except for the distal area between the moraines A and C, where large piled boulders occur. These sorted debris stripes range from 1 to 5 m in length and their depth below the ground varies from a few centimeters to at least 1 m. These debris-filled stripes do not have a prevailing orientation. They spread randomly on the ground and tend to occur on both low and high terrain.

A prominent oval-shaped landform stands out ~30 m from the surrounding hummocky terrain. It is ~500 m long, ~450 m wide, and located ~1.5 km from the current glacier front. It is flanked by the two main streams of the valley (Fig. 2). Distally, this landform merges with the surrounding topography. On its surface, sub-angular, sub-rounded, and rounded cobbles and boulders occur. Some of these are large boulders embedded in the surface (>2 m in height), which in turn are faceted and striated. Debris-filled stripes in the ground appear towards the flanks of this prominent landform. These alignments of debris can reach up to 3 m in length (Fig. 4b) and 1–4 m in width. Debris-filled sinkholes also occur (Fig. 6c). Additionally, throughout the landform surface, glacial lineations coincident with the ice flow direction are observed in the satellite images (Fig. 2).

4.1.3. Flutes

Flutes are ubiquitous in the middle section of the UNI IV moraine complex, where they are superimposed onto the hummocky terrain dominating the forefield. Some of these flutes are distinct and preserved as elongated ridges composed of matrix-supported sub-rounded and rounded granodioritic pebbles (Fig. 7a). The flutes are ~1 m in height, decreasing gradually to their distal margin, and their lengths vary from 10 to more than 80 m. Generally, the flutes develop on the lee-side of well-polished and striated boulders (Fig. 7b, d). Less well-formed flutes, with discrete conic sediment accumulation on the lee

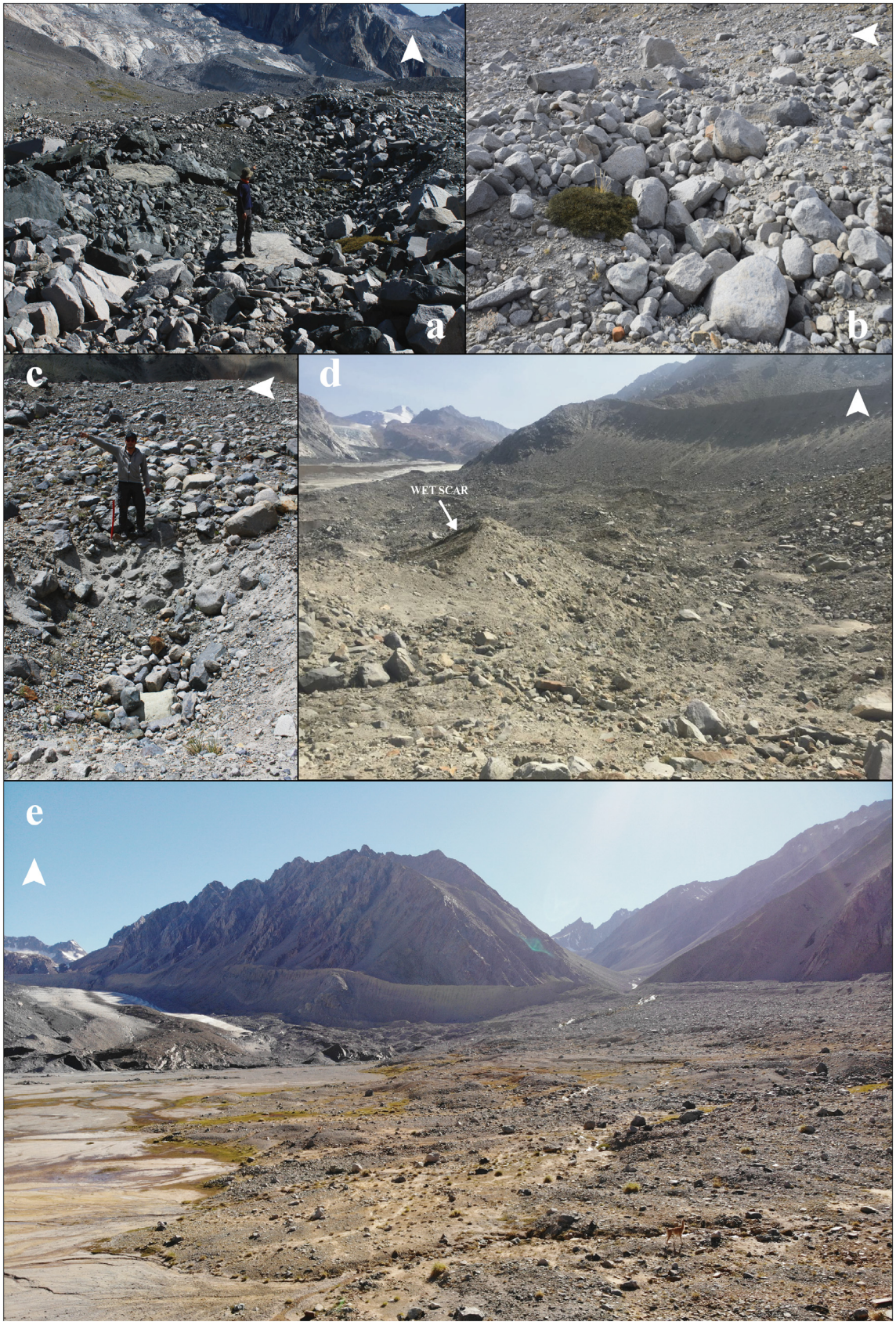

Fig. 6. Geomorphological attributes of hummocky terrain. **(a)** Sinkholes in the frontal, distal margin of the UNI V complex between moraines A-B; **(b)** Sorted debris stripes in the ground and **(c)** sinkholes on the flank of basal till plain; **(d)** Eastern margin of the Universidad Glacier ablation zone; note the wet scars and overall irregular debris-covered ice topography; **(e)** Panoramic view of the forefield near the main active outwash plain. Also, the picture shows, in the background, the main lateral section of moraine B. White arrows point out the North.

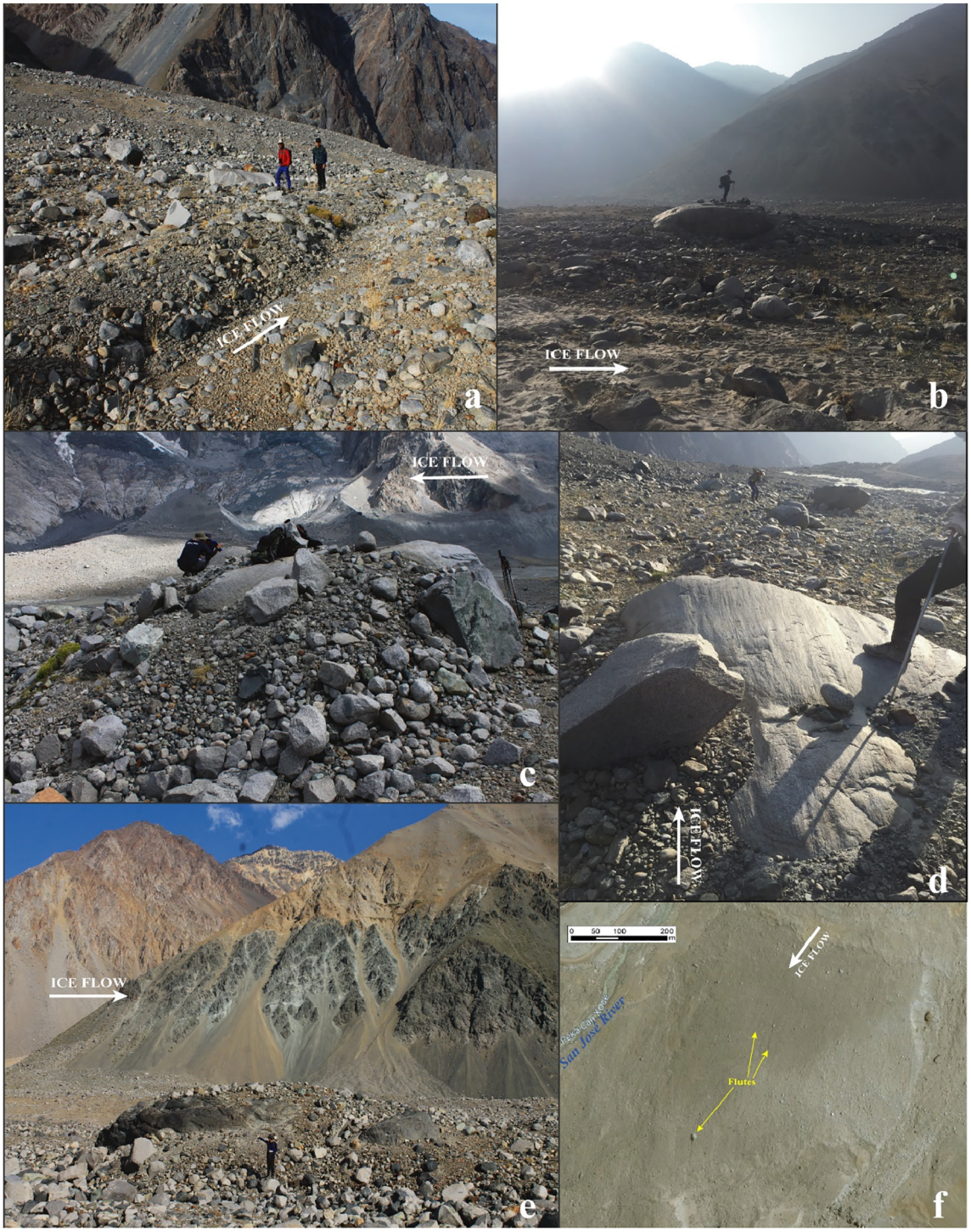

Fig. 7. Different types of glacial flutes on the hummocky terrain. **(a)** Flute composed of sub-rounded and rounded granodioritic matrix-supported debris between moraines D_2 and E. The view is to the south; **(b)** Profile view of a flute developed on the lee-side of a roche moutonnée boulder; **(c, e)** Large boulders covered with a patchy debris veneer on the surface and with an unconsolidated sedimentary tail; **(d)** Down-glacier view of a flute. The person in the foreground is standing on the flute; **(f)** Aerial view of the flutes overriding the large basal till plain (oval-shaped landform).

sides of the big boulders, appear covered by a patchy debris veneer on their surface (Fig. 7c, e). This debris veneer resembles poorly consolidated melt-out sediment composed of angular to rounded material.

Flutes occur in swaths between moraines B and F (Fig. 2). Flutes between moraines C and D_1 are spatially distributed in two distinct groups. Group one includes at least twelve flutes near the eastern margin of the forefield. They are no more than 10 m apart and show a 135° azimuth (Fig. 2). The second group of flutes occurs over the prominent oval-shaped landform. There are more than thirty flutes spaced 10–30 m apart with a 210° azimuth. While it was not possible to distinguish this last set of flutes during fieldwork, they were identified using satellite imagery, which recorded smooth and narrow flutes of up to 80 m in length (Fig. 7f). Another set of flutes occurs between moraines E and F (Fig. 2). This set of flutes consists of about thirty units spaced 3–20 m apart. These flutes also have a 210° azimuth and, due to their exceptional preservation, can be identified easily in the field (Fig. 7a, b).

4.2. The debris-covered glacier snout

The Universidad Glacier ablation zone extends from ~3700 to ~2500 m a.s.l. (Bravo et al., 2017). The lower area of the glacier is characterized by extensive debris cover at the margins (Figs. 1, 2). This is particularly evident towards the eastern side of the glacier as it approaches the lateral moraines, where debris cover seems thicker. The poorly consolidated debris cover ranges from 0.1–2 m in thickness. A recognizable medial moraine, formed by merging the Manke and Universidad Glaciers, emerges over the surrounding ice (Fig. 8a). Transversal sediment ridges appear on the glacier surface (Fig. 8b). These ridges reach ~3 m in height and are composed of fines and granodiorite rounded and sub-rounded pebbles. Ice cliffs punctuate the whole ablation area near the ice front, as high as 7 m with slopes over 40° (Fig. 8c). Stacked granodiorite cobbles are commonly found with boulders, forming gravity cones at the bases of ice cliffs. The accumulated debris includes rounded or sub-rounded shapes with an absence of fine material on the surface, which likely has been washed out. The continuous stacking of debris at the bases of ice cliffs promotes the formation of talus that commonly reaches the tops of the cliffs, covering them totally.

The area close to the eastern lateral moraine exhibits a hummocky topography without visible ice on the surface (Fig. 8d). Here, it is possible to recognize debris-filled stripes and sinkholes. Fractures on the slope of the hummocks range from a few cm to ~6 m in length and are not more than 1.5 m wide. Large debris usually falls into the fractures,

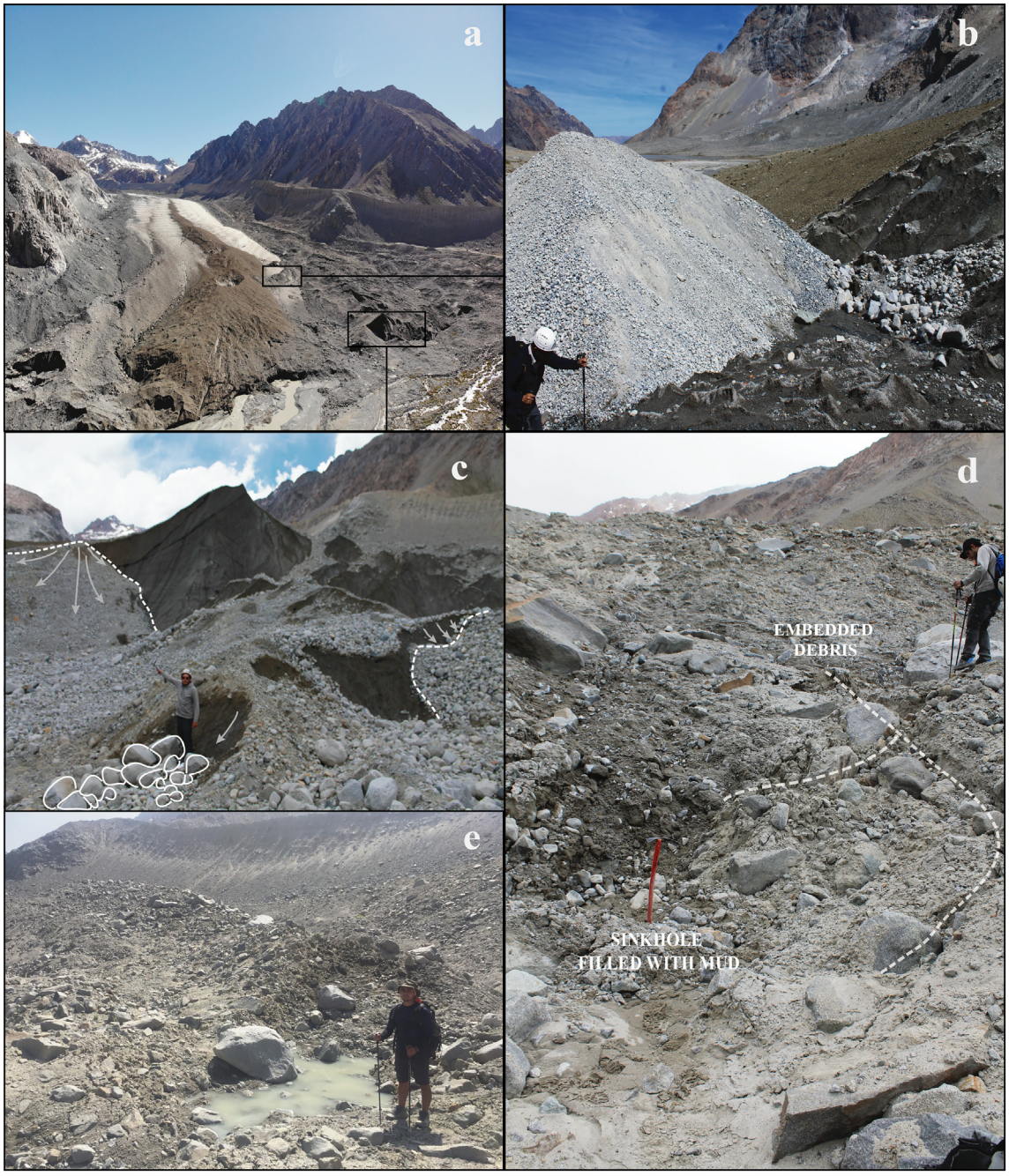

Fig. 8. The debris-covered glacier snout. **(a)** Up-glacier view of the ablation zone. The boxes indicate the location of images (b) and (c); **(b)** Crevasse-squeeze ridges on the glacier front; **(c)** Ice cliff and movement of sediment due to backwasting; **(d)** Tension cracks and sinkhole formation where ice is debris-covered; **(e)** Melt-out pond over the glacier debris-covered flank.

which are subsequently arranged in linear patterns, embedded in the ground (Fig. 8d). This process gives, in some cases, a debris-striped ground appearance.

Active supraglacial sinkholes, formed in response to underlying ice melting, occur in the debris-covered glacier snout. They usually have mud and/or water at their bottoms, indicating that the ice is melting *in-situ*. Overall, these sinkholes reach a width of 3 m and a depth of 3 m into the glacier, and they resemble those described in the hummocky terrain (see section 4.1.2). A common process observed is the sliding of debris (pebble to boulder size) along the slopes of hummocks towards the bottoms of sinkholes. This debris movement produces wet scars on the slopes of the hummocks (Fig. 6d).

Small melt-out ponds are scattered over the debris-covered ablation zone. They never exceed a diameter of 5 m or a depth of 1.5 m (Fig. 8e). Sandy patches are also common in the ablation zone, probably as a result of the desiccation of these ponds. Turbulent supraglacial meltwater streams occur in the clean ice, and reach the subglacial zone and the forefield at some point.

In brief, the geomorphology of the ablation zone is characterized by an extensive debris cover producing a mostly irregular topography near the ice front and towards the lateral moraines A-D (Fig. 2). Most of these topographic features have been forming during that last 40 years, as observed in the available remote-sensing imagery. Ice cliffs are frequent and disrupt the local topography. Here, mass wasting, such as the sliding of debris along the slopes of the terrain, occurs. Towards the glacier flanks, no ice is exposed. Debris-filled stripes, debris-filled sinkholes, and dry or water-filled melt-out ponds are present throughout the ice-covered surface.

4.3. Geochronology

Four ^{10}Be-dated erratic boulder samples were obtained from the top of moraine B. Three of them were sampled from the eastern lateral margin (UNI 1801, UNI1802, and UNI1803) and one from the frontal ridge (UNI1903) (Fig. 2). Complementarily, two boulders were sampled from the flute field between moraines D_2 and E (UNI1904 and UNI1905) (Fig. 2). The three boulders sampled from the lateral margin of moraine B yielded exposure ages of 240 ± 40, 330 ± 50, and 665 ± 150 years, respectively. The other boulder sampled from the frontal ridge of moraine B yielded an exposure age of 470 ± 100 years. The two samples retrieved from boulders on the flute field between moraines D_2 and E yielded exposure ages of 360 ± 50 and 460 ± 100 years (Table 1; Fig. 2), respectively. These are all young ages that are close to the lower limit of the ^{10}Be method. Consequently, the analytical errors are relatively high.

5. Discussion

In this section, we discuss the morphogenesis and general geochronologic context of landforms studied in the forefield of the Universidad Glacier (*i.e.*, the UNI IV moraine complex). We interpret the geomorphic record to reveal the type of deglaciation that occurred during the latest Holocene period and to provide the context for the interpretation of the present de-icing trend. In order to put our results in a more global context, we analyze our geomorphological interpretations in comparison to work carried out in other regions experiencing glacier recession.

5.1. Timing of morphogenesis

Taken at face value, the ^{10}Be exposure dating suggests an overall deglacial trend during the last 665 ± 150 years, interrupted by multiple ice stabilization or re-advance phases. The outer ridges of moraines A-C correspond to the maximum latest Holocene glacier extent. The ice flow that built up moraines D_1, D_2, and E in the middle of the forefield represents an intermediate glacier extension until the first half of the 20th century. The final ice snout stabilization or re-advance is observed with moraines F and G, which indicate the latest standstill/re-advance of the ice front during the second half and end of the 20th century. Since then, the glacier has only declined.

5.2. Active ice derived landforms

Together with the eight moraine ridges mapped in the Universidad Glacier forefield, the flutes also indicate an actively flowing temperate-based glacier (Boulton, 1976; Gordon et al., 1992; Benn and Evans, 2014). Distinguishing whether moraines represent ice front standstill or re-advances is not possible at this time. Regarding the flutes, we identified two groups parallel to the main valley axis and a third perpendicular to the lateral moraine ridges (D, C, B) (Fig. 2). Flutes have not been described previously in the literature for the Central Andes of Chile, but they have been observed in the forefield of the Juncal Sur Glacier (33° S; J.-L. García, field observations). We mapped two types of flutes with different heights and lengths (Fig. 7). Both types occur intercalated, for instance, in the flute field between moraines D_1 and F (Fig. 2). As the flutes occur superimposed on the massive hummocky terrain, it is assumed that sediments from the latter were reworked into the flutes during active glacier flow. The flutes are composed of glacially polished clasts in the diamict that indicates their subglacial genesis. According to Boulton (1976) and Gordon et al. (1992), flutes accurately indicate the former direction of the ice flow, as they are produced by the abrasion and quarrying of subglacial boulders. Evans (2014) suggested that the glacier-bed coupling should generate similar flute sizes during discrete glacial events. It is possible that the sets of flutes that occur between moraines C—D_1 and *E*-F are linked to different glacial standstill and/or expansion events and, thereby, expose discrete times of active ice flow.

Lliboutry (1958) suggested that there must have been a "glacier flood" of the Universidad Glacier in the first half of the 20th century. The ice field extended 1 km further down-valley in 1944 when compared to 1956. Consequently, some authors started to report glacier surge events in Central Chile during the mid-20th century, including at the Universidad Glacier (Falaschi et al., 2018; Iturrizaga and Charrier, 2021).

Glacier surges refer to episodes where ice is rapidly transported from an upper reservoir zone to the receiving area in the lower glacier, owing to internal dynamic instabilities (Meier and Post, 1969; Evans and Rea, 1999; Benn and Evans, 2014; Bhambri et al., 2017; Benn, 2021). Surging glaciers are commonly recognizable by their geomorphic signatures. Diagnostic surge landforms summarized by Evans and Rea (1999) and Ingólfsson et al. (2016) include thrust-block moraines and push moraines; crevasse-squeeze ridges on the forefield; concertina ice-cored eskers; long flutes; hummocky moraine belts; pitted outwash; extensive dead ice fields; and drumlins. These landforms alone cannot be attributed to glacier surging without a landsystem approach (Evans and Rea, 1999; Evans et al., 2009; Evans, 2014; Benn, 2021). Surging glaciers have been well documented, particularly in Arctic (Evans and Rea, 1999; Evans et al., 2009; Evans, 2011; Schomacker et al., 2014; Ingólfsson et al., 2016) and alpine environments (Sutherland et al., 2019; Benn, 2021). The UNI IV moraine complex has some of the diagnostic elements of surging ice, such as flutes. However, thrust-block moraines, push moraines, and crevasse-squeeze ridges within the forefield have not been identified. The sinuous shape of moraine F might be interpreted as concertina esker with a subglacial origin. However, this differs from descriptions that suggest englacial and/or supraglacial origins of concertina eskers during a surging event (Evans and Rea, 1999; Schomacker et al., 2014; Ingólfsson et al., 2016). Besides, a concertina ice-cored esker produced by a surging glacier should have poor preservation potential due to deposition and subsequent melting of dead ice (Evans and Rea, 1999). Additionally, the UNI IV moraine complex does not show hummocky moraine belts or pitted outwash. Therefore, the dead ice present in the glacier margin is not a consequence of a prior surging glacier, but the result of gradual evolution from active to stagnant ice.

The geomorphologic record of putative surging glaciers in the Central Andes remains unknown. According to the available literature of surging glaciers and the landforms mapped on the UNI IV moraine complex, surging events are not evident. We recommend further sedimentological analysis of moraine F or the well-preserved flutes of moraine E to establish whether these landforms are associated with a glacier re-advance or surge. Moreover, we consider it necessary to improve our understanding of potential surge events in the Central Andes through a regional landsystem approach.

5.3. Stagnant ice-derived landforms

Deglacial features located between moraines suggest that after a phase of glacial standstill/expansion, a period of mostly *in situ* ice decay took place. The large hummocky terrain contains micro- and meso-scale geomorphologic structures that are best explained by an *in situ* collapse of debris-covered ice (Kjær and Krüger, 2001). Thus, the hummocky terrain is interpreted as the final product of the melting of buried and inactive ice (Benn, 1992; Benn and Evans, 2014). This process implies that after a glacier standstill/advance, the ice front stagnates and becomes debris-covered, leading to geomorphic features associated with dead ice melting. The differential ablation (Eyles, 1979; Mölg et al., 2020) forms the irregular topography that we observe as the hummocky terrain, including the formation of sinkholes and debris-filled stripes. These features have been largely described as a consequence of progressive *in situ* de-icing at present-day glacier margins (Krüger et al., 2010) and of past deglaciation in dead ice topography records (Schomacker, 2007; Crump et al., 2017).

The UNI IV moraine complex exposes irregular topography with 3–4 m relief, particularly towards the frontal margins of the outer moraine ridges (A-C). This chaotic accumulation of debris is punctuated by large depressions that can be best interpreted as inactive sinkholes (Krüger and Kjær, 2000). Morphogenesis of sinkholes in Iceland and the high Arctic is related to dead ice melting (Kjær and Krüger, 2001; Schomacker and Kjær, 2008). According to these authors, the space left by the thaw of the sediment-covered dead ice bodies generates subsidence, producing sinkholes. These hollows are often filled with debris at their bottoms due to sediment gravity flows triggered by the gradual melting of surrounding buried ice. Water or mud deposits at the sinkhole bottoms indicate local water saturation on the ground, originating from the melting of buried ice (Kjær and Krüger, 2001). The production of sinkholes and melt-out ponds ends when the melting of the buried ice ceases or when water drains through ice fractures during the thawing phase. Sinkholes were also reported in the debris-covered glaciers of the Himalayas, where they were interpreted as resulting from the collapse of englacial conduits (Benn et al., 2017; Dobreva et al., 2017). In the Central Andes of Chile, sinkholes are common in present-day debris-covered glaciers and in the latest Holocene glacial geomorphic record (Bodin et al., 2010; García et al., 2014).

The aforementioned fractures are also evidence of *in situ* ice decay. Eyles (1979), Kjær and Krüger (2001), and Schomacker and Kjær (2008) suggested that the gradual decay of buried mostly inactive ice bodies promotes the development of tension cracks above the frozen terrain. Then, pebbles, cobbles, and boulders fill the tension cracks. This process promotes the formation of debris-filled stripes in the ground. The debris-filled stripes vary from place to place depending on the past or present degradation of ice-cored moraines (Eyles, 1979; Kjær and Krüger, 2001). In the UNI IV moraine complex, we found debris-filled stripes that varied from centimeters to meters (see section 4.1.2), suggesting melt-out of dead ice. Debris-filled stripes stand out and are widespread between moraines D-G, denoting progressive *in situ* de-icing (Fig. 6b). The deglacial geomorphology described here has also been recorded in subpolar and polar regions (Schomacker, 2007; Crump et al., 2017) as a product of latest Holocene de-icing. The reports match debris-filled stripes with the degradation of ice-cored moraines or the collapse of dead ice bodies (Krüger and Kjær, 2000; Krüger et al., 2010).

The interpretation of the oval-shaped landform in the southwest section of the forefield (Fig. 2) is more difficult. It may be linked to a prior and longer stagnant phase of the glacier front. During the stagnation phase, the rate of debris accumulation might have been higher than the evacuation to the glaciofluvial system, triggering the vertical deformation of the ice snout. Similar processes have been described by Eyles and Rogerson (1978) on Austerdalsbreen in Norway; van Woerkom et al. (2019) on Lirung Glacier, a Nepalese debris-covered glacier; and recently by Mölg et al. (2020) on the Zmuttgletscher, a debris-covered glacier in Switzerland. Our interpretation also follows the geomorphological observations made by Iturrizaga and Charrier (2021), who reported the presence of a prominent hummocky terrain deposit in the Chilean Cachapoal Valley (34° S) linked to former dead ice disintegration. According to Iturrizaga and Charrier (2021), that hummocky terrain was overridden by recent re-advances of Cachapoal Glacier. The oval-shaped landform that occurs in the forefield of the Universidad Glacier includes sinkholes (Fig. 6c) and debris-filled stripes in the ground (Fig. 4b) that reflect the de-icing process. Thus, the oval-shaped landform may be part of the relief formed during the development of moraines A-B. After its deposition, this landform was overridden subglacially, similar to what occurred in Cachapoal Valley.

The top of the overridden till plain has various elongated features (Fig. 7f). It is possible that some of these features are flutes produced by the ice flow at the time the moraine C was formed. However, other elongated features record the effect of subtle meltwater linear erosion when the ice stood at moraine D_1 on the proximal side of this oval-shaped landform. Today, the oval-shaped landform is flanked on both sides by meltwater streams, one of which is the San José River draining the Universidad Glacier (Fig. 2). Glacioflucial erosion has also increased the landform's prominence.

5.4. Current deglaciation

The Universidad Glacier ablation zone exhibits features of glacier front stagnation and *in situ* degradation of ice under a debris layer, as described in other works in the region (García et al., 2014; Janke et al., 2015). Geomorphic features demonstrate this condition, such as the conspicuous transversal outcrop ridges of sediments composed of rounded pebbles and fines appearing on the ice surface (Fig. 8b). This sediment is likely to be crevasse-squeeze ridges that attest to shear in the ice margin (Evans and Twigg, 2002; Benn and Evans, 2014). Crevasse-squeeze ridges have been associated with the movement of the upper, active flow of the glacier as it overrides the slow-moving or stagnant ice front (Phillips et al., 2017). This would be connected to the formation of dead ice bodies on the lower section of the glacier during the de-icing process (Kjær and Krüger, 2001). Thus, one deglaciation characteristic is the presence of active (upper-glacier) ice flowing down-valley over stagnant ice that has already separated or started to separate (García et al., 2014).

In addition, the ice cliffs present in the marginal zone might be understood as part of the active/inactive transition of debris-covered glaciers (Watson et al., 2017). The origin of such ice cliffs remains mostly unexplored (Mölg et al., 2020), although some authors suggest that their formation is linked to the overriding dynamics of active ice over inactive ice (Krüger et al., 2010). The ice cliffs are melting chiefly through backwasting, the principal ablation factor of debris-covered glaciers (Krüger and Kjær, 1999; Schomacker and Kjær, 2008; Sakai et al., 2000; Reid and Brock, 2014; Ewertowski and Tomczyk, 2015). Backwasting consumes the vertical clean ice, triggering two results: remobilization of debris and more irregular topography (Krüger et al., 2010; Mölg et al., 2020). Therefore, the presence of ice cliffs in the ablation zone is another feature reflecting the current deglaciation of the stagnant Universidad Glacier snout.

According to Eyles (1979) and Krüger et al. (2010), sinkholes are associated with the presence of ice bodies below a reworked supraglacial till. Local melting of isolated and buried ice cores triggers ground subsidence (Krüger and Kjær, 2000). Sinkholes and melt-out ponds can be considered landforms inherited from the current deglaciation. Ultimately, debris-filled stripes in the ground denote debris-filled tension cracks formed during the de-icing of the stagnant ice (Kjær and Krüger, 2001). The surface lowering due to ice melting produces other topographic features, including wet scars on the hummocks' slopes. The geomorphic record in the Universidad Glacier's ablation zone indicates that the *in situ* ice-decay is associated with a stagnant ice front that best characterizes the present-day response to climate warming and drying (García et al., 2014; Janke et al., 2015; Charrier et al., 2019; Iturrizaga and Charrier, 2021).

5.5. De-icing conceptual model

The geomorphological record of the Universidad Glacier is associated with glacier standstills/advances, glacier front stagnation, the transition to debris-covered ice, and finally, degradation into ice-cored moraines. Thus, the melting of isolated dead ice bodies leads to the dead ice moraine (*sensu* Kjær and Krüger, 2001; Schomacker and Kjær, 2007; Krüger et al., 2010) with a massive ice-free hummocky topography that is preserved along this upper Central Andean catchment (Janke et al., 2015; Charrier et al., 2019; Iturrizaga and Charrier, 2021). Based on our findings, we develop the following de-icing model for the Universidad Glacier, which also represents other glaciers of the region (Fig. 9):

- After an ice advance (Fig. 9a), long periods of negative mass balance trigger the glacier front to stagnate, be covered by debris, and downswaste (Fig. 9b). The movement of active ice onto the inactive glacier front triggers intense shearing in the transitional zone. This produces crevasse-squeezed ridges and ice cliffs. The supraglacial sediment layer gets thicker as ice-downwaste sediment emerges through thrust planes. Mass wasting on the valley's sides and lateral moraines also occurs (Curry et al., 2006; Janke et al., 2015). Once the local exposed ice, such as in ice cliffs, is completely debris-covered, the supraglacial layer thickness determines the de-icing progress and resultant geomorphology.
- The debris-covered ice snout becomes an ice-cored moraine detached from the active glacier (Fig. 9c). The ice-cored terrain degradation produces identifiable landform features such as i) hummocky topography; ii) sinkholes with their bottoms filled by debris; iii) tension cracks in the inner slopes; iv) debris-filled stripes in the ground; and v) meltwater in melt-out ponds. These features have been described as part of the disintegration of ice-cored moraines (Kjær and Krüger, 2001; Schomacker and Kjaer, 2007) following a stagnant phase of debris-covered ice. We observe these features at different locations, such as between moraines A-D. The geomorphological features described above were also observed in the degradation of dead-ice bodies by García et al. (2014) in the Central Andes of Chile; Krüger et al. (2010) in subpolar environments; and Benn et al. (2017) in the Himalayas.
- After de-icing of buried ice has ended, the ice-free hummocky terrain or dead-ice moraine is produced and remains as the deglacial record. The ice-free hummocky topography has been described as part of the geomorphology of the upper catchment in the Central Andes of Chile and Argentina (Wayne and Corte, 1983; Bodin et al., 2010; García et al., 2014; Janke et al., 2015; Charrier et al., 2019; Iturrizaga and Charrier, 2021), but without the morphogenetic interpretation we provide here.

The deglaciation process of the Universidad Glacier has not been linear during the last 665 ± 150 years, but interrupted by ice standstills/re-advances until very recently. Flutes within moraines C and D are evidence of active flowing ice. Glacier activity near the mid-20th century, represented by moraine E, also left flutes. Since then, the ice has collapsed, and the glacier has had short standstills or pulses (moraines F and G). Therefore, a complete deglaciation model for the latest Holocene period needs to include this dynamic nature of active and inactive ice phases in the Central Andes of Chile (Fig. 9d-e).

6. Conclusions

The geomorphology of the forefield of the Universidad Glacier is a mosaic of glacial and deglacial landforms, that exposes a juxtaposition of morphogenetic ice processes acting over the past 665 ± 150 years. The main geomorphic deglacial features we observe are sinkholes and debris-filled stripes in the ground within a bouldery, hummocky relief surface. These features, along with ice cliffs, crevasse-squeeze ridges, melt-out ponds, and debris-infilled sinkholes, indicate an inactive ice phase we observe in present-day Universidad Glacier. On the other side, we identified eight moraine belts and flutes that emerge from the UNI IV moraine complex, evidence of active ice flow and sediment transport/rework during the overall ice decay period until very recently (the end of the 20th century).

A debris-rich environment such as the Central Andes of Chile affects the ice front during warming climate conditions: a stagnant buried ice body evolves. The transition from active ice to inactive buried ice during deglaciations is expected to occur each time the climate warms and dries, as we observe today at the Universidad Glacier. Intercalated colder and wetter climate regimes will promote a composite geomorphic record like that recorded by the UNI IV moraine complex.

A heuristic model for the latest Holocene glacial and deglacial phase for the Universidad Glacier, and likely other glaciers in the Central Andes of Chile, includes three stages: (I) main glacier expansion within the last 665 ± 150 years (moraine A) and subsequent ice front stagnation associated with a rich debris cover leading to the development of ice-cored and finally dead-ice moraines; (II) glacier front retreat interrupted by multiple standstill/re-advances that overrode and reworked former glacial deposits, producing landforms such as flutes and inner moraine ridges; and (III) the current deglaciation, which repeats the de-icing process described in Stages I and II.

Under the current warming and drying trends in the Central Andes of Chile (Barcaza et al., 2017; Garreaud et al., 2020), a negative mass balance of glaciers will continue to result in increased debris coverage and gradual loss of ice under a thick debris mantle. The relevance of these glaciers as essential water resources in the Central Andes of Chile contrasts with the lack of work dedicated to the Andean cryosphere. We thus suggest that further studies associated with the depth, volume, rate and manner of deglaciation in the Central Andes are urgently needed to build a comprehensive regional understanding of glacier-climate interactions. The Universidad Glacier can be a starting point for interpreting the latest Holocene de-icing dynamics of the other glaciers in this region. Furthermore, additional sedimentological investigations would improve our understanding of standstill/advance periods and their relationship to the presence or absence of surge-type glaciers.

Declaration of competing interest

The authors declare that they have no known competing financial interests or personal relationships that could have appeared to influence the work reported in this paper.

Acknowledgments

The authors acknowledge Sebastián Ruiz Pereira, Diego Romero, and Brandon Navarro for their contributions during fieldwork. We thank Carla Rivera, Chantel Register, and Gabrielle Vance for their editing suggestions. We are indebted to Arturo Troncoso and Roberto Frank

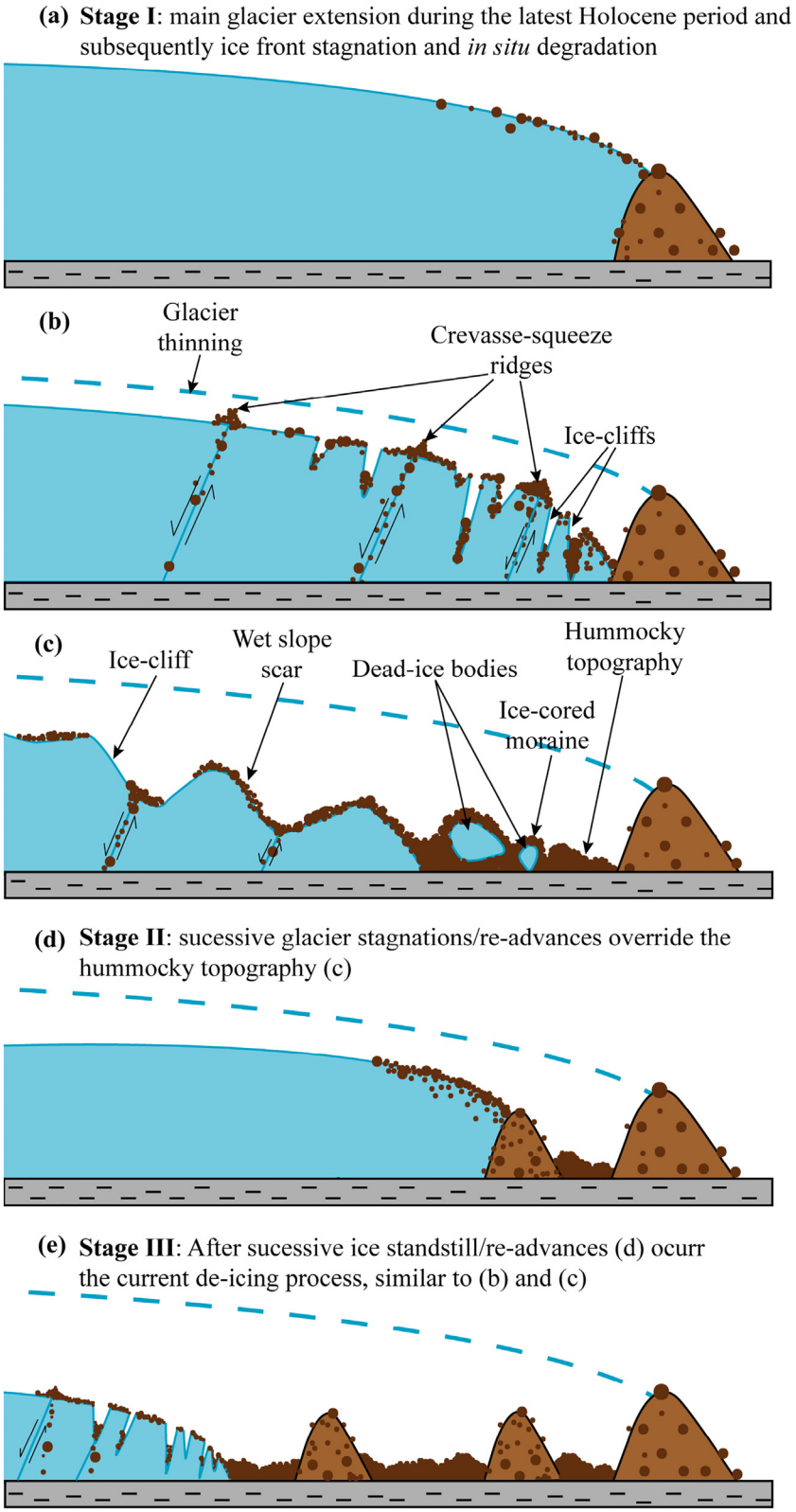

Fig. 9. De-icing model for the Universidad Glacier. Stage I: **(a)** main glacier extension during the latest Holocene period **(b)** During the de-icing process, the glacier front becomes stagnant and thinner. As a result, the ice surface is covered with debris; **(c)** The debris-covered glacier front undergoes differential ablation and ice-cored moraines are developed; **Stage II (d)** successive glacier stagnations/re-advances override the forefield; **Stage III (e)** Current de-icing. The main implication of the landsystem including glacial and deglacial features is that the current de-icing process seems to be mimicking what occurred after the main late Holocene advance (moraines A-B).

for facilitating our access to the study area. We sincerely thank the hydropower station, San Andrés, which gave us support in our research with their workspaces. Additionally, we appreciate Naki Akçar for providing the ultra-pure ^{9}Be carrier. Finally, we are indebted to two anonymous reviewers and their suggestions on an earlier version of the manuscript.

This research was funded by the Chilean National Agency for Research and Development (ANID)/scholarship program/Doctorado Nacional/21171594, FONDECYT #1200935 awarded to J.-L.G, and the Seed Money Grant from the Leading House for the Latin American Region, University of St. Gallen, Switzerland awarded to S.U.N. and J.-L.G., FONDECYT grant #3170869 and a Hanse-Wissenschaftskolleg junior Fellowship to A.J.G.

Appendix A. Supplementary data

Supplementary data to this article can be found online at https://doi.org/10.1016/j.geomorph.2021.108096.

References

Abraham, E.M., Rodríguez, M.D., Rubio, M.C., Guida-Johnson, B., Gomez, L., Rubio, C., 2020. Disentangling the concept of "South American Arid Diagonal". J. Arid Environ. 175, 104089. https://doi.org/10.1016/j.jaridenv.2019.104089.

Ayala, A., Pellicciotti, F., MacDonell, S., McPhee, J., Vivero, S., Campos, C., Egli, P., 2016. Modelling the hydrological response of debris-free and debris-covered glaciers to present climatic conditions in the semiarid Andes of central Chile. Hydrol. Process. https://doi.org/10.1002/hyp.10971.

Azócar, G.F., Brenning, A., 2010. Hydrological and geomorphological significance of rock glaciers in the dry Andes, Chile (27°-33°S). Permafr. Periglac. Process. 21, 42–53. https://doi.org/10.1002/ppp.669.

Balco, G., Stone, J.O., Lifton, N.A., Dunai, T.J., 2008. A complete and easily accessible means of calculating surface exposure ages or erosion rates from 10 Be and 26 Al measurements. Quat. Geochronol. 3, 174–195. https://doi.org/10.1016/j.quageo.2007.12.001.

Ballantyne, C.K., 1995. Paraglacial debris-cone formation on recently deglaciated terrain, western Norway. The Holocene 5, 25–33. https://doi.org/10.1177/095968369500500104.

Ballantyne, C.K., 2002. Paraglacial geomorphology. Quat. Sci. Rev. 21, 1935–2017. https://doi.org/10.1016/S0277-3791(02)00005-7.

Ballantyne, C.K., 2008. After the ice: Holocene geomorphic activity in the Scottish Highlands. Scott. Geogr. J. https://doi.org/10.1080/14702540802300167.

Barcaza, G., Nussbaumer, S., Tapia, G., Valdés, J., García, J.L., Videla, Y., Albornoz, A., Arias, V., 2017. Glacier inventory and recent glacier variations in the Andes of Chile, South America. Ann. Glaciol. 58, 166–180. https://doi.org/10.1017/aog.2017.28.

Barsch, D., Liedtke, H., 1980. Principles, scientific value and practical applicability of the geomorphological map of the Federal Republic of Germany at the scale 1:50000 (GMK 25) and 1:100000 (GMK 100). Z.Geomorphol.Suppl.Issues 296–313.

Bellisario, A., Ferrando, F., Janke, J., 2013. Water resources in Chile: the critical relation between glaciers and mining for sustainable water management. Investig.Geogr.Chile 46, 3–24.

Benn, D.I., 1992. The genesis and significance of "hummocky moraine": evidence from the Isle of Skye, Scotland. Quat. Sci. Rev. 11, 781–799. https://doi.org/10.1016/0277-3791(92)90083-K.

Benn, D.I., 2021. Surging glaciers in Scotland. Scott. Geogr. J., 1–40 https://doi.org/10.1080/14702541.2021.1922738.

Benn, D.I., Evans, D.J.A., 2014. Glaciers And Glaciation. Second. ed. Routledge, London https://doi.org/10.4324/9780203785010.

Benn, D.I., Owen, L., 2002. Himalayan glacial sedimentary environments: a framework for reconstructing and dating the former extent of glaciers in high mountains. Quat. Int. 97–98, 3–25. https://doi.org/10.1016/S1040-6182(02)00048-4.

Benn, D.I., Thompson, S., Gulley, J., Mertes, J., Luckman, A., Nicholson, L., 2017. Structure and evolution of the drainage system of a Himalayan debris-covered glacier, and its relationship with patterns of mass loss. Cryosphere 11, 2247–2264. https://doi.org/10.5194/tc-11-2247-2017.

Bennett, M.R., Huddart, D., Glasser, N.F., Hambrey, M.J., 2000. Resedimentation of debris on an ice-cored lateral moraine in the high-Arctic (Kongsvegen, Svalbard). Geomorphology 35, 21–40. https://doi.org/10.1016/S0169-555X(00)00017-9.

Bhambri, R., Hewitt, K., Kawishwar, P., Pratap, B., 2017. Surge-type and surge-modified glaciers in the Karakoram. Sci. Rep. 7, 1–14. https://doi.org/10.1038/s41598-017-15473-8.

Bodin, X., Rojas, F., Brenning, A., 2010. Status and evolution of the cryosphere in the Andes of Santiago (Chile, 33.5°S.). Geomorphology 118, 453–464. https://doi.org/10.1016/j.geomorph.2010.02.016.

Boulton, G.S., 1976. The origin of glacially fluted surfaces-observations and theory. J. Glaciol. 17, 287–309. https://doi.org/10.3189/S0022143000013605.

Bravo, C., Loriaux, T., Rivera, A., Brock, B.W., 2017. Assessing glacier melt contribution to streamflow at Universidad Glacier, central Andes of Chile. Hydrol. Earth Syst. Sci. 21, 3249–3266. https://doi.org/10.5194/hess-21-3249-2017.

Brenning, A., 2005. Geomorphological, hydrological and climatic significance of rock glaciers in the Andes of Central Chile (33–35°S). Permafr. Periglac. Process. 16, 231–240. https://doi.org/10.1002/ppp.528.

Buri, P., Miles, E.S., Steiner, J.F., Ragettli, S., Pellicciotti, F., 2021. Supraglacial ice cliffs can substantially increase the mass loss of debris-covered glaciers. Geophys. Res. Lett. 48. https://doi.org/10.1029/2020GL092150.

Charrier, R., Lillo, F., 1973. Geología regional y geoquímica del drenaje de las provincias de O'Higgins y Colchagua. Instituto de Investigaciones de Recursos Naturales, Santiago.

Charrier, R., Iturrizaga, L., Carretier, S., Regard, V., 2019. Geomorphologic and glacial evolution of the Cachapoal and southern Maipo catchments in the Andean Principal Cordillera, central Chile (34 ° -35o S). Andean Geol. 46, 240–278. https://doi.org/10.5027/andgeoV46n2-3108.

Chmeleff, J., von Blanckenburg, F., Kossert, K., Jakob, D., 2010. Determination of the 10 Be half-life by multicollector ICP-MS and liquid scintillation counting. Nucl. Instrum. Methods Phys. Res. Sect. B 268, 192–199. https://doi.org/10.1016/j.nimb.2009.09.012.

Christl, M., Vockenhuber, C., Kubik, P.W., Wacker, L., Lachner, J., Alfimov, V., Synal, H.A., 2013. The ETH Zurich AMS facilities: performance parameters and reference materials. Nucl. Instrum. Methods Phys. Res. Sect. B 294, 29–38. https://doi.org/10.1016/j.nimb.2012.03.004.

Clayton, L., 1964. Karst topography on stagnant glaciers. J. Glaciol. 5, 107–112. https://doi.org/10.3189/S0022143000028628.

Crump, S.E., Anderson, L.S., Miller, G.H., Anderson, R.S., 2017. Interpreting exposure ages from ice-cored moraines: a Neoglacial case study on Baffin Island, Arctic Canada. J. Quat. Sci. 32, 1049–1062. https://doi.org/10.1002/jqs.2979.

Curry, A.M., Cleasby, V., Zukowskyj, P., 2006. Paraglacial response of steep, sediment-mantled slopes to post-'Little Ice Age' glacier recession in the central Swiss Alps. J. Quat. Sci. 21, 211–225. https://doi.org/10.1002/jqs.954.

Dirección General de Aguas, 2014. Catastro nacional de glaciares. Unidad de Glaciología y Nieves, Dirección General de Aguas. Ministerio de Obras Públicas.

Dobreva, I., Bishop, M., Bush, A., 2017. Climate–glacier dynamics and topographic forcing in the Karakoram Himalaya: concepts, issues and research directions. Water 9, 405. https://doi.org/10.3390/w9060405.

Eichel, J., Draebing, D., Meyer, N., 2018. From active to stable: paraglacial transition of Alpine lateral moraine slopes. Land Degrad. Dev. 29, 4158–4172. https://doi.org/10.1002/ldr.3140.

Evans, D.J.A., 2009. Controlled moraines: origins, characteristics and palaeoglaciological implications. Quat. Sci. Rev. 28, 183–208. https://doi.org/10.1016/j.quascirev.2008.10.024.

Evans, D.J.A., 2011. Glacial landsystems of Satujökull, Iceland: a modern analogue for glacial landsystem overprinting by mountain icecaps. Geomorphology 129, 225–237. https://doi.org/10.1016/j.geomorph.2011.01.025.

Evans, D.J.A., 2014. Glacial Landsystems. 1st ed. Routledge https://doi.org/10.4324/9780203784976.

Evans, D.J.A., Rea, B.R., 1999. Geomorphology and sedimentology of surging glaciers: a land-systems approach. Ann. Glaciol. 28, 75–82.

Evans, D.J.A., Twigg, D.R., 2002. The active temperate glacial landsystem: a model based on Breiðamerkurjökull and Fjallsjökull, Iceland. Quat. Sci. Rev. 21, 2143–2177. https://doi.org/10.1016/S0277-3791(02)00019-7.

Evans, D.J.A., Twigg, D.R., Rea, B.R., Orton, C., 2009. Surging glacier landsystem of Tungnaárjökull, Iceland. J.Maps 5, 134–151. https://doi.org/10.4113/jom.2009.1064.

Ewertowski, M.W., Tomczyk, A.M., 2015. Quantification of the ice-cored moraines' short-term dynamics in the high-Arctic glaciers Ebbabreen and Ragnarbreen, Petuniabukta, Svalbard. Geomorphology 234, 211–227. https://doi.org/10.1016/j.geomorph.2015.01.023.

Eyles, N., 1979. Facies of supraglacial sedimentation on Icelandic and Alpine temperate glaciers. Can. J. Earth Sci. 16, 1341–1361. https://doi.org/10.1139/e79-121.

Eyles, N., Rogerson, R.J., 1978. A framework for the investigation of medial moraine formation: Austerdalsbreen, Norway, and Berendon Glacier, British Columbia, Canada. J. Glaciol. 20, 99–113. https://doi.org/10.3189/s0022143000021249.

Falaschi, D., Bolch, T., Lenzano, M.G., Tadono, T., Lo Vecchio, A., Lenzano, L., 2018. New evidence of glacier surges in the Central Andes of Argentina and Chile. Prog.Phys.Geogr. EarthEnviron. 42, 792–825. https://doi.org/10.1177/0309133318803014.

Fernández, H., Ferrando, F., 2018. Glaciares rocosos en la zona semiárida de Chile: relevancia de un recurso hídrico sin protección normativa. Cuad.Geogr.Rev.Colomb. Geogr. 27, 338–355. https://doi.org/10.15446/rcdg.v27n2.63370.

García, J.-L., Pizarro, F., Calcagni, V., 2014. Fluctuaciones glaciales holocénicas en el Cajón del Maipo, Andes centrales de Chile: observaciones morfoestratigráficas de los glaciares Loma Larga y Nieves Negras. In: GEOlibros (Ed.), Los Riesgos Traen Oportunidades. Transformaciones Globales En Los Andes Sudamericanos. Instituto de Geografía de la Pontificia Universidad Católica de Chile, Santiago, pp. 35–52.

Garreaud, R.D., 2009. The Andes climate and weather. Adv. Geosci. 7, 1–9.

Garreaud, R.D., Boisier, J.P., Rondanelli, R., Montecinos, A., Sepúlveda, H.H., Veloso-Aguila, D., 2020. The Central Chile Mega Drought (2010–2018): a climate dynamics perspective. Int. J. Climatol. 40, 421–439. https://doi.org/10.1002/joc.6219.

Glasser, N.F., Hambrey, M.J., 2002. Sedimentary facies and landform genesis at a temperate outlet glacier: soler glacier, North Patagonian Icefield. Sedimentology 49, 43–64. https://doi.org/10.1046/j.1365-3091.2002.00431.x.

Gordon, J.E., Brian Whalley, W., Gellatly, A.F., Vere, D.M., 1992. The formation of glacial flutes: assessment of models with evidence from Lyngsdalen, North Norway. Quat. Sci. Rev. 11, 709–731. https://doi.org/10.1016/0277-3791(92)90079-N.

Gosse, J.C., Phillips, F.M., 2001. Terrestrial in situ cosmogenic nuclides:theory and application. Quat. Sci. Rev. 20, 1475–1560. https://doi.org/10.1016/S0277-3791(00)00171-2.

Hambrey, M.J., Quincey, D.J., Glasser, N.F., Reynolds, J.M., Richardson, S.J., Clemmens, S., 2008. Sedimentological, geomorphological and dynamic context of debris-mantled glaciers, Mount Everest (Sagarmatha) region,Nepal. Quat. Sci. Rev. 27, 2361–2389. https://doi.org/10.1016/j.quascirev.2008.08.010.

Hugonnet, R., McNabb, R., Berthier, E., Menounos, B., Nuth, C., Girod, L., Farinotti, D., Huss, M., Dussaillant, I., Brun, F., Kääb, A., 2021. Accelerated global glacier mass loss in the early twenty-first century. Nature 592, 726–731. https://doi.org/10.1038/s41586-021-03436-z.

Ingólfsson, Ó., Benediktsson, Í.Ö., Schomacker, A., Kjær, K.H., Brynjólfsson, S., Jónsson, S.A., Korsgaard, N.J., Johnson, M.D., 2016. Glacial geological studies of surge-type glaciers in Iceland - research status and future challenges. Earth Sci. Rev. 152, 37–69. https://doi.org/10.1016/j.earscirev.2015.11.008.

Iturrizaga, L., Charrier, R., 2021. Sudden glacier advances in the Cachapoal Valley, Southern Central Andes of Chile (34°S). J. S. Am. Earth Sci. 105, 102787. https://doi.org/10.1016/j.jsames.2020.102787.

Janke, J.R., Bellisario, A.C., Ferrando, F.A., 2015. Classification of debris-covered glaciers and rock glaciers in the Andes of central Chile. Geomorphology 241, 98–121. https://doi.org/10.1016/j.geomorph.2015.03.034.

Jones, D.B., Harrison, S., Anderson, K., 2019. Mountain glacier-to-rock glacier transition. Glob. Planet. Chang. 181, 102999. https://doi.org/10.1016/j.gloplacha.2019.102999.

Kaplan, M.R., Strelin, J.A., Schaefer, J.M., Denton, G.H., Finkel, R.C., Schwartz, R., Putnam, A.E., Vandergoes, M.J., Goehring, B.M., Travis, S.G., 2011. In-situ cosmogenic 10 Be production rate at Lago Argentino, Patagonia: implications for late-glacial climate chronology. Earth Planet. Sci. Lett. 309, 21–32. https://doi.org/10.1016/j.epsl.2011.06.018.

King, O., Turner, A.G.D., Quincey, D.J., Carrivick, J.L., 2020. Morphometric evolution of Everest region debris-covered glaciers. Geomorphology 371, 107422. https://doi.org/10.1016/j.geomorph.2020.107422.

Kjær, K.H., Krüger, J., 2001. The final phase of dead-ice moraine development: processes and sediment architecture, Kötlujökull, Iceland. Sedimentology 48, 935–952.

Kneisel, C., 1988. Legende für geomorphologische Kartierungen in Hochgebirgen (GMK Hochgebirge). - Trierer Geographische Studien, p. 18.

Kohl, C.P., Nishiizumi, K., 1992. Chemical isolation of quartz for measurement of in-situ-produced cosmogenic nuclides. Geochim. Cosmochim. Acta 56, 3583–3587.

Korschinek, G., Bergmaier, A., Faestermann, T., Gerstmann, U.C., Knie, K., Rugel, G., Wallner, A., Dillmann, I., Dollinger, G., von Gostomski, C.L., Kossert, K., Maiti, M., Poutivtsev, M., Remmert, A., 2010. A new value for the half-life of 10Be by heavy-ion elastic recoil detection and liquid scintillation counting. Nucl. Instrum. Methods Phys. Res. Sect. B 268, 187–191. https://doi.org/10.1016/j.nimb.2009.09.020.

Krüger, J., Kjær, K.H., 1999. A data chart for field description and genetic interpretation of glacial diamicts and associated sediments - with examples from Greenland, Iceland, and Denmark. Boreas 28, 386–402. https://doi.org/10.1111/j.1502-3885.1999.tb00228.x.

Krüger, J., Kjær, K.H., 2000. De-icing progression of ice-cored moraines in a humid, subpolar climate, Kötlujökull, Iceland. Holocene 10, 737–747. https://doi.org/10.1191/09596830094980.

Krüger, J., Kjær, K.H., Schomacker, A., 2010. Dead-ice environments: a landsystems model for a debris-charged, stagnant lowland glacier margin, Kötlujökull. Developments in Quaternary Science, pp. 105–126 https://doi.org/10.1016/S1571-0866(09)01307-4.

Lal, D., 1991. Cosmic ray labeling of erosion surfaces: in situ nuclide production rates and erosion models. Earth Planet. Sci. Lett. 104, 424–439. https://doi.org/10.1016/0012-821X(91)90220-C.

Le Quesne, C., Acuña, C., Boninsegna, J.A., Rivera, A., Barichivich, J., 2009. Long-term glacier variations in the Central Andes of Argentina and Chile, inferred from historical records and tree-ring reconstructed precipitation. Palaeogeogr. Palaeoclimatol. Palaeoecol. 281, 334–344. https://doi.org/10.1016/j.palaeo.2008.01.039.

Lliboutry, L., 1958. Studies of the shrinkage after a sudden advance, blue bands and wave ogives on Glaciar Universidad (Central Chilean Andes). J. Glaciol. 3, 261–270.

Lliboutry, L., 1998. Glaciers of Chile and Argentina. In: Richards, W., Ferrigno, J. (Eds.), Satellite Image Atlas of Glaciers of the World - South America. U.S. Geological Survey, Washington D.C., p. 229.

Lukas, S., Nicholson, L.I., Ross, F.H., Humlum, O., 2005. Formation, meltout processes and landscape alteration of high-arctic ice-cored moraines - examples from Nordenskiöld land, central Spitsbergen. Polar Geogr. 29, 157–187. https://doi.org/10.1080/789610198.

Lukas, S., Nicholson, L.I., Humlum, O., 2007. Comment on Lønne and Lyså (2005): "Deglaciation dynamics following the Little Ice Age on Svalbard: implications for shaping of landscapes at high latitudes", Geomorphology 72, 300–319. Geomorphology 84, 145–149. https://doi.org/10.1016/j.geomorph.2006.07.003.

Mackintosh, A.N., Anderson, B.M., Pierrehumbert, R.T., 2017. Reconstructing climate from glaciers. Annu. Rev. Earth Planet. Sci. 45, 649–680. https://doi.org/10.1146/annurev-earth-063016-020643.

Malmros, J.K., Mernild, S.H., Wilson, R., Yde, J.C., Fensholt, R., 2016. Glacier area changes in the central Chilean and Argentinean Andes 1955–2013/14. J. Glaciol. 62, 391–401. https://doi.org/10.1017/jog.2016.43.

Meier, M.F., Post, A., 1969. What are glacier surges? Can. J. Earth Sci. 6, 807–817. https://doi.org/10.1139/e69-081.

Mölg, N., Ferguson, J., Bolch, T., Vieli, A., 2020. On the influence of debris cover on glacier morphology: how high-relief structures evolve from smooth surfaces. Geomorphology 357, 107092. https://doi.org/10.1016/j.geomorph.2020.107092.

Monnier, S., Kinnard, C., 2017. Pluri-decadal (1955–2014) evolution of glacier–rock glacier transitional landforms in the central Andes of Chile (30–33° S). Earth Surf.Dyn. 5, 493–509. https://doi.org/10.5194/esurf-5-493-2017.

Nishiizumi, K., Imamura, M., Caffee, M.W., Southon, J.R., Finkel, R.C., McAninch, J., 2007. Absolute calibration of 10 Be AMS standards. Nucl. Instrum. Methods Phys. Res. Sect. B 258, 403–413. https://doi.org/10.1016/j.nimb.2007.01.297.

Oliva, M., Ruiz-Fernández, J., 2015. Coupling patterns between para-glacial and permafrost degradation responses in Antarctica. Earth Surf. Process. Landf. 40, 1227–1238. https://doi.org/10.1002/esp.3716.

Owen, L.A., 1991. Mass movement deposits in the Karakoram Mountains: their sedimentary characteristics, recognition and role in Karakoram landform evolution. Z. Geomorphol. 35, 401–424.

Patterson, C.J., 1998. Laurentide glacial landscapes: the role of ice streams. Geology 26, 643. https://doi.org/10.1130/0091-7613(1998)026<0643:LGLTRO>2.3.CO;2.

Phillips, E., Everest, J., Evans, D.J.A., Finlayson, A., Ewertowski, M., Guild, A., Jones, L., 2017. Concentrated, 'pulsed' axial glacier flow: structural glaciological evidence from Kviárjökull in SE Iceland. Earth Surf. Process. Landf. 42, 1901–1922. https://doi.org/10.1002/esp.4145.

Reid, T.D., Brock, B.W., 2014. Assessing ice-cliff backwasting and its contribution to total ablation of debris-covered Miage glacier, Mont Blanc massif, Italy. J. Glaciol. 60, 3–13. https://doi.org/10.3189/2014JoG13J045.

Sakai, A., Takeuchi, N., Fujita, K., Nakawo, M., 2000. Role of supraglacial ponds in the ablation process of a debris-covered glacier in the Nepal Himalayas. Debris-covered Glaciers.IAHS, Seattle, Washington, pp. 119–130

Schomacker, A., 2007. Dead-ice Under Different Climate Conditions: Processes, Landforms, Sediments And Melt Rate in Iceland And Svalbard. Lund University.

Schomacker, A., 2008. What controls dead-ice melting under different climate conditions? A discussion. Earth Sci. Rev. 90, 103–113. https://doi.org/10.1016/j.earscirev.2008.08.003.

Schomacker, A., Kjaer, K.H., 2007. Origin and de-icing of multiple generations of ice-cored moraines at Brúarjökull, Iceland. Boreas 36, 411–425. https://doi.org/10.1080/03009480701213554.

Schomacker, A., Kjær, K.H., 2008. Quantification of dead-ice melting in ice-cored moraines at the high-Arctic glacier Holmströmbreen, Svalbard. Boreas 37, 211–225. https://doi.org/10.1111/j.1502-3885.2007.00014.x.

Schomacker, A., Benediktsson, Í.Ö., Ingólfsson, Ó., 2014. The Eyjabakkajökull glacial landsystem, Iceland: geomorphic impact of multiple surges. Geomorphology 218, 98–107. https://doi.org/10.1016/j.geomorph.2013.07.005.

SERNAGEOMIN, 2004. Mapa geológico de Chile: versión digital 1:1.000.000.

Shroder, J.F., Bishop, M.P., Copland, L., Sloan, V.F., 2000. Debris-covered glaciers and rock glaciers in the Nanga Parbat Himalaya, Pakistan. Geogr.Ann.Ser.APhys.Geogr. 82, 17–31. https://doi.org/10.1111/j.0435-3676.2000.00108.x.

Stone, J.O., 2000. Air pressure and cosmogenic isotope production. J.Geophys.Res.Solid Earth 105, 23753–23759. https://doi.org/10.1029/2000JB900181.

Sutherland, J.L., Carrivick, J.L., Evans, D.J.A., Shulmeister, J., Quincey, D.J., 2019. The Tekapo Glacier, New Zealand, during the Last Glacial Maximum: an active temperate glacier influenced by intermittent surge activity. Geomorphology 343, 183–210. https://doi.org/10.1016/j.geomorph.2019.07.008.

Swift, D.A., Cook, S.J., Graham, D.J., Midgley, N.G., Fallick, A.E., Storrar, R., Toubes Rodrigo, M., Evans, D.J.A., 2018. Terminal zone glacial sediment transfer at a temperate overdeepened glacier system. Quat. Sci. Rev. 180, 111–131. https://doi.org/10.1016/j.quascirev.2017.11.027.

Watson, C.S., Quincey, D.J., Smith, M.W., Carrivick, J.L., Rowan, A.V., James, M.R., 2017. Quantifying ice cliff evolution with multi-temporal point clouds on the debris-covered Khumbu Glacier,Nepal. J. Glaciol. 63, 823–837. https://doi.org/10.1017/jog.2017.47.

Wayne, W., Corte, A., 1983. Multiple glaciations of the Cordon del Plata, Mendoza Argentina. Palaeogeogr. Palaeoclimatol. Palaeoecol. 42, 185–209.

Wilson, R., Mernild, S.H., Malmros, J.K., Bravo, C., Carrión, D., 2016. Surface velocity fluctuations for Glaciar Universidad, central Chile, between 1967 and 2015. J. Glaciol. 62, 847–860. https://doi.org/10.1017/jog.2016.73.

van Woerkom, T., Steiner, J.F., Kraaijenbrink, P.D.A., Miles, E.S., Immerzeel, W.W., 2019. Sediment supply from lateral moraines to a debris-covered glacier in the Himalaya. Earth Surf.Dyn. 7, 411–427. https://doi.org/10.5194/esurf-7-411-2019.